J. Vis. Commun. Image R. xxx (2009) xxx–xxx

Contents lists available at ScienceDirect

J. Vis. Commun. Image R.

journal homepage: www.elsevier.com/locate/jvci

Geometric algebra colour image representations and derived total orderings for morphological operators – Part I: Colour quaternions

Jesús Angulo *

CMM – Centre de Morphologie Mathématique, Mathématiques et Systèmes, MINES Paristech, 35, rue Saint Honoré, 77305 Fontainebleau Cedex, France

ARTICLE INFO

Article history:
Received 21 October 2008
Available online xxxx

Keywords:
Colour mathematical morphology
Colour quaternion
Quaternion total ordering
Nonlinear colour filtering
Colour feature extraction
Colour image representation
Hypercomplex representation
Colour potential function
Quaternion complete lattice

ABSTRACT

The definition of morphological operators for colour images requires a total ordering for colour points. A colour can be represented by different algebraic structures, in this paper we focus on real quaternions. The paper presents two main contributions. On the one hand, we have studied different alternatives to introduce the scalar part to obtain full colour quaternions. On the other hand, several total lexicographic orderings for quaternions have been defined, according to the various quaternion decompositions. The properties of these quaternionic orderings have been characterised to enable the identification of the most useful ones to define colour morphological operators. The theoretical results are illustrated with examples of processed images which show the usefulness of the proposed operators for real life complex problems.

1. Introduction

Mathematical morphology is the application of lattice theory to spatial structures. This means that the definition of morphological operators needs a totally ordered complete lattice structure, i.e., the possibility of defining an ordering relationship among the points to be processed. Considering the case of colour images, let $\mathbf{c}_i = (r_i, g_i, b_i)$ be the triplet of the red, green and blue intensities for the pixel i of a digital colour image, and let $\leqslant_\Omega$ be a total ordering between the colour points, i.e., for any pair of unequal points $\mathbf{c}_i$ and $\mathbf{c}_j$ it should be possible to verify if $\mathbf{c}_i \leqslant_\Omega \mathbf{c}_j$ or if $\mathbf{c}_i \geqslant_\Omega \mathbf{c}_j$. For any subset of RGB points, its colour erosion (dilation) is defined as the infimum (supremum) according to $\leqslant_\Omega$. In other words, $(\mathscr{T}^{rgb}, \leqslant_\Omega)$ is a complete lattice. The challenge in the extension of mathematical morphology to colour images is just the definition of appropriate total colour orderings. For a general account on mathematical morphology the interested reader should refer to the two pioneer books by Serra [37] and to an excellent monograph by Heijmans [21]. Fundamental references to works which have studied the theory of vector morphology theory are [38,17,42]. Many approaches have been proposed in the last few years on the extension of mathematical morphology to colour images. An exhaustive state-of-the-art has been reported in recent papers by Angulo [5] and by Aptoula and Lefévre [6].

This paper is the first part of a series of studies which focus on defining colour total orderings based on geometric algebra representations of colour images. In particular, in this article we focus on real quaternions, or hypercomplex numbers, as discovered by Hamilton in 1843 [18]. In the forthcoming second paper, we will consider the case of colour tensors and derived total orderings. We explore here the way to build colour quaternions from a RGB triplet and the different alternatives to define total orderings based on the specific properties of two quaternion representations (polar form and parallel/perpendicular decomposition), characterising and identifying the most useful to define nonlinear morphological operators. The theoretical results are illustrated with examples of processed images.

Colour images can be represented according to three main families of colour spaces: "3 primaries-based" spaces (e.g. RGB, XYZ, etc.), "1 intensity + 2 chrominances" spaces (e.g., YUV, $L^*a^*b^*$, etc.), and "luminance/saturation/hue 3d-polar" spaces (e.g., HLS, HSV, LSH [4], etc.). The reader interested in standard colour space representation is invited to the books of reference [45,33]. In this study we focus specifically in the RGB representation, which in fact is the most direct way to manipulate digital colour images, for three main reasons: (1) colour images are produced in RGB representation by most of digital devices; (2) the three R, G and B channels can be considered as a three dimensional vectorial space, which constitutes a fundamental starting point for geometric algebra formalisation; (3) application of multivariate data analysis techniques such as principal component analysis (PCA), etc. allow to reduce the dimension of multispectral images, and in most of cases the n image channels can be represented in 3 PCA axis.

* Fax: +33 1 64 69 47 07.
E-mail addresses: jesus.angulo@ensmp.fr, angulo@cmm.ensmp.fr.

1047-3203/$ - see front matter © 2009 Elsevier Inc. All rights reserved.
doi:10.1016/j.jvcir.2009.10.002

A colour point $\mathbf{c}_i$ can be represented according to different geometric algebra structures. Di Zenzo [9] proposed in his pioneer work a tensor representation of colour derivatives in order to compute the colour gradient by considering the colour image as a surface in $\mathbb{R}^3$. Later, Sochen and Zeevi [40] and Sochen et al. [41] considered a colour image as a two-dimensional manifold embedded in the five-dimensional non-Euclidean space, whose coordinates are $(x, y, R, G, B) \in \mathbb{R}^5$, which is described by Beltrami colour metric tensor. But all these studies consider only the differential representation of the colour triplet, which is useful for differential geometric colour processing, e.g., colour image enhancement and smoothing using PDE. Another algebraic tool used to represent and to perform colour transformations by taking into account the 3D vector nature of colour triplets is the quaternion. The first application of quaterion colour processing was reported by Sangwine [34] for computing a Fourier colour transform. Other quaternionic colour transformations were then explored by Sangwine and Ell such as colour image correlation [10], colour convolution for linear filtering [36] and for vector edge-detecting [35] as well as new results on quaternion Fourier transforms of colour images [11]. Ell [13] introduced recently the application of quaternion linear transformations of colour images (e.g., rotation and reflections of colours). Other works by Denis et al. [8] and Carré and Denis [7] have also explored new approaches for colour spectral analysis, edge detection and colour wavelet transform. Quaternion representations have been also used to define colour statistical moments and derived applications by Pei and Cheng [31] and to build colour Principal Component Analysis [32,26,39]. Quaternion algebra can be generalised in terms of Clifford algebra. In this last framework, Labunets et al. have studied Fourier colour transform [24], including colour wavelets for compression and edge detection, as well as computation of invariants of nD colour images [23,25]. Ell [14] has also started to study this representations for colour convolution and Fourier transform.

All this previous work on colour quaternions deals with linear colour transformations of colour images. Our purpose here is to explore how colour quaternion representation can be useful for non-linear inf and sup colour processing. To our knowledge this is the first work considering the definition of colour mathematical morphology using quaternions, and more generally, the first to define total ordering between quaternions.

The rest of the paper is organised as follows. In Section 2 we discuss the colour quaternion representation, considering the various alternatives to define the scalar part of a full colour quaternion. Then, in Section 3 we present the total orderings introduced for colour quaternions, including a study of their invariance properties and a comparison with more classical colour total orderings. Morphological operators for colour images are defined in Section 4. The behaviour and the applications of morphological colour filters using quaternion orderings are illustrated in Section 5. Finally, the conclusion and perspectives are given in Section 6.

1.1. Notation for RGB colour images

Let $f(\mathbf{x})$ be a greylevel image, $f : E \to \mathcal{T}$, in that case $\mathcal{T} = \{t_{min}, t_{min}+1, \ldots, t_{max}\}$ (in general $\mathcal{T} \subset \mathbb{Z}$ or $\mathbb{R}$, for our study $\mathcal{T} \equiv [0,1]$) is an ordered set of grey-levels and typically, for the digital 2D images $\mathbf{x} = (x, y) \in E$ where $E \subset \mathbb{Z}^2$ is the support of the image. We denote by $\mathcal{F}(E, \mathcal{T})$ the functions from E onto $\mathcal{T}$. If $\mathcal{T}$ is a complete lattice, then $\mathcal{F}(E, \mathcal{T})$ is a complete lattice too. Given the three sets of scalar values $\mathcal{T}^r, \mathcal{T}^g, \mathcal{T}^b$, we denote by $\mathcal{F}(E, [\mathcal{T}^r \times \mathcal{T}^g \times \mathcal{T}^b])$ or $\mathcal{F}(E, \mathcal{T}^{rgb})$, with $\mathcal{T}^r = \mathcal{T}^g = \mathcal{T}^b \equiv [0,1]$, all colour images in a red/green/blue representation. We denote the elements of $\mathcal{F}(E, \mathcal{T}^{rgb})$ by $\mathbf{f}$, where $\mathbf{f} = (f_R, f_G, f_B)$ are the colour component functions. Using this representation, the value of $\mathbf{f}$ at a point $\mathbf{x} \in E$, which lies in $\mathcal{T}^{rgb}$, is denoted by $\mathbf{f}(\mathbf{x}) = (f_R(\mathbf{x}), f_G(\mathbf{x}), f_B(\mathbf{x}))$.

Each of the N pixels of a colour image ($N = card(E)$) corresponds to a colour point $\mathbf{c}_i = (r_i, g_i, b_i)$ of the colour space $\mathscr{C} \equiv [0,1] \times [0,1] \times [0,1]$, such as $\mathbf{c}_i = \mathbf{f}(\mathbf{x}_i) = (f_R(\mathbf{x}_i), f_G(\mathbf{x}_i), f_B(\mathbf{x}_i))$ and where $1 \leqslant i \leqslant N$.

2. Colour quaternion image representations

2.1. From RGB points to colour quaternions: the choice of the scalar part

A quaternion $\mathbf{q} \in \mathbb{H}$ may be represented in hypercomplex form as

$$\mathbf{q} = a + bi + cj + dk, \tag{1}$$

where a, b, c and d are real. A quaternion has a *real part or scalar part*, $S(\mathbf{q}) = a$, and an *imaginary part or vector part*, $V(\mathbf{q}) = bi + cj + dk$, such that the whole quaternion may be represented by the sum of its scalar and vector parts as $\mathbf{q} = S(\mathbf{q}) + V(\mathbf{q})$. A quaternion with a zero real/scalar part is called a *pure quaternion*. The algebra of quaternions, and in particular the definition of the product of two quaternions, may be found in standard graduate texts on applied mathematics.

According to the previous works on the representation of colour by quaternions, we consider the grey-centered RGB colour-space [10]. In this space, the unit RGB cube is translated so that the coordinate origin $\widehat{O}(0,0,0)$ represents mid-grey (middle point of the grey axis or half-way between black and white). Then, a colour can be represented by a pure quaternion: $\mathbf{c} = (r, g, b) \Rightarrow \mathbf{q} = \hat{r}i + \hat{g}j + \hat{b}k$, where $\hat{\mathbf{c}} = (\hat{r}, \hat{g}, \hat{b}) = (r - 1/2, g - 1/2, b - 1/2)$. It should be remarked that in this centered RGB colour space the black colour quaternion and the white colour quaternion, associated to the two main achromatic colours, play a symmetrical role in terms of distance to the center and the same is true for any pair of complementary colours.

In order to better exploit the power of quaternion algebra, we propose here to introduce a scalar part for each colour quaternion, i.e.,

$$\mathbf{c} = (r, g, b) \;\Rightarrow\; \mathbf{q} = \psi(\mathbf{c}, \mathbf{c}_0) + \hat{r}i + \hat{g}j + \hat{b}k. \tag{2}$$

The scalar component, $\psi(\mathbf{c}, \mathbf{c}_0)$, is a real value obtained from the current colour point and a colour of reference $\mathbf{c}_0 = (r_0, g_0, b_0)$. As we will show, the scalar part provides the structure to introduce an additional datum which can be a colour magnitude, a distance or a potential. The choice of the reference colour is an interesting degree of freedom to impose to each colour an "ordering" with respect to this outer colour, and consequently an effect of the operator favouring a particular colour.

We have considered three possible definitions for the scalar part.

2.1.1. Saturation

$$\psi(\mathbf{c}_i, \mathbf{c}_0)^{sat} = s_i - 1/2 = -\frac{1}{2} + \begin{cases} \frac{3}{2}(max_i - m_i) & \text{if } m_i \geqslant med_i \\ \frac{3}{2}(m_i - min_i) & \text{if } m_i \leqslant med_i, \end{cases} \tag{3}$$

where $m_i = (r_i + g_i + b_i)/3, max_i = \max(r_i, g_i, b_i), min_i = \min(r_i, g_i, b_i)$ and med_i is the median value of the triplet (r_i, g_i, b_i). In fact, s_i is the saturation of the luminance/saturation/hue representation in norm L_1 [4], obtained as the modulus of the projected colour vector on the chromatic plane (i.e., the orthogonal plane to the grey axis in the origin). The saturation in norm L_1 can be also written as

Please cite this article in press as: J. Angulo, Geometric algebra colour image representations and derived total orderings for morphological operators – Part I: Colour quaternions, J. Vis. Commun. (2009), doi:10.1016/j.jvcir.2009.10.002

$$s_i = \frac{1}{4}(|2r_i - g_i - b_i| + |2g_i - r_i - b_i| + |2b_i - r_i - g_i|). \quad (4)$$

The luminance l_i in norm L_1 is the average value of intensities, i.e.,

$$l_i = m_i = \frac{1}{3}(r_i + g_i + b_i). \quad (5)$$

Keep in mind these colour magnitudes which will appear below in colour quaternion decompositions. Obviously, the value of saturation for $\mathbf{c}_i$ does not depend on the reference colour $\mathbf{c}_0$. The saturation s_i is the chromatic variety of a colour (i.e., the degree of dilution, inverse to the quantity of "white" of the colour) and it cannot be obtained as a simple linear combination of RGB values in contrast to the luminance l_i. This is the rationale behind the appropriateness of $\psi(\mathbf{c}_i, \mathbf{c}_0)^{sat}$ as scalar value for the colour quaternion. We notice that in the scalar part the saturation defined in [0,1] has been centered in order to have a symmetrical 4D space $[-0.5, 0.5] \times [-0.5, 0.5] \times [-0.5, 0.5] \times [-0.5, 0.5]$.

2.1.2. Mass with respect to $\mathbf{c}_0$

$$\psi(\mathbf{c}_i, \mathbf{c}_0)_{\lambda}^{mass} = exp\left(-w_E\|\mathbf{c}_i - \mathbf{c}_0\| - w_{\angle}\arccos\left(\frac{\langle \mathbf{c}_i, \mathbf{c}_0\rangle}{\|\mathbf{c}_i\|\|\mathbf{c}_0\|}\right)\right), \quad (6)$$

where $w_E = (1/\sqrt{2})\lambda$ and $w_{\angle} = (2\pi)^{-1}(1-\lambda)$. It is a decreasing function of a linear barycentric combination of two colour distances between $\mathbf{c}_i$ and the reference colour $\mathbf{c}_0$. The value of $0 \leqslant \lambda \leqslant 1$ allows to weigh up the influence of the Euclidean distance (i.e., RGB uniform distance) between both colours with respect to the angle distance (i.e., chromatic distance equivalent to a hue distance). Consequently, the value of the scalar component $\psi(\mathbf{c}_i, \mathbf{c}_0)_{\lambda}^{mass}$ is maximal for $\mathbf{c}_i = \mathbf{c}_0$ and decreases when the colour $\mathbf{c}_i$ gets away from the reference $\mathbf{c}_0$. In any case, the values are always positive and can be normalised in order to have the same dynamics as the colour quaternion complex components.

2.1.3. Potential with respect to $\mathbf{c}_0$ and the nine significant colour points in the RGB unit cube

$$\psi(\mathbf{c}_i, \mathbf{c}_0)^{pot} = \phi_E^+ + \phi_E^- = \frac{\kappa^+}{4\pi\epsilon_0\|\mathbf{c}_i - \mathbf{c}_0\|} + \sum_{n=-4,\ n\neq i}^{4} \frac{\kappa^-}{4\pi\epsilon_0\|\mathbf{c}_i - \mathbf{c}^n\|}, \quad (7)$$

where the positive potential ϕ_E^+ represents the influence of a positive charge placed at the position of the reference colour $\mathbf{c}_0$ and the negative term ϕ_E^- corresponds to the potential associated to nine negative charges in the significant colours of the cube $\mathscr{C}$. These significant colours are the main achromatic colours (black $\mathbf{c}^{-1} = (0,0,0)$, mid-grey $\mathbf{c}^0 = (1/2, 1/2, 1/2)$ and white $\mathbf{c}^1 = (1,1,1)$), the chromatic primaries (red $\mathbf{c}^2 = (1,0,0)$, green $\mathbf{c}^3 = (0,1,0)$ and blue $\mathbf{c}^4 = (0,0,1)$), and the chromatic complementary primaries (cyan $\mathbf{c}^{-2} = (0,1,1)$, magenta $\mathbf{c}^{-3} = (1,0,1)$ and yellow $\mathbf{c}^{-4} = (1,1,0)$). This function $\psi(\mathbf{c}_i, \mathbf{c}_0)^{pot}$ balances the influence of the reference point with respect to the significant points of the RGB cube. Typically, to equilibrate both kinds of charges, it is taken $\kappa^+ = 9Q$ and $\kappa^- = -Q$, and in order to make the computation easier we fix $Q = \mu/(4\pi\epsilon_0)$. The value of constant μ allows to control the dynamics of this scalar part with respect to the other quaternion components.

2.2. Colour quaternion representations

Besides the hypercomplex representation, we are considering in this paper two other interesting quaternion representations.

2.2.1. Colour quaternion polar form

Any quaternion may be represented in polar form as

$$\mathbf{q} = \rho e^{\xi\theta}, \quad (8)$$

with $\rho = \sqrt{a^2 + b^2 + c^2 + d^2}$, $\xi = \frac{bi+cj+dk}{\sqrt{b^2+c^2+d^2}} = \overline{\xi}_i i + \overline{\xi}_j j + \overline{\xi}_k k$ and $\theta = \arctan\left(\frac{\sqrt{b^2+c^2+d^2}}{a}\right)$. Then, a quaternion can be rewritten in a trigonometric version as $\mathbf{q} = \rho(\cos\theta + \xi\sin\theta)$.

In this polar formulation, $\rho = |\mathbf{q}|$ is the modulus of $\mathbf{q}$; ξ is the pure unitary quaternion associated to $\mathbf{q}$ (by the normalisation, the quaternion representation of a colour discards distance information, but retains orientation information relative to mid-grey, which correspond in fact to the chromatic or hue-related information.), sometimes called *eigenaxis*; and θ is the angle, sometimes called *eigenangle*, between the real part and the 3D imaginary part.

The eigenaxis of a colour quaternion, ξ, is independent from its scalar part. The imaginary term $\mu = b^2 + c^2 + d^2 = (r - 1/2)^2 + (g - 1/2)^2 + (b - 1/2)^2$ is the norm of the colour vector in the centered cube and can be considered as a perceived energy of the colour (i.e., relative energy with respect to the mid-grey), being maximal for the eight significant colours associated to the cube corners. Note that the black and white have the same value as the six chromatic colours. The modulus ρ is an additive combination of the imaginary part and the scalar part. The function arctan (four-quadrant inverse tangent) is defined in the interval $[-\pi/2, \pi/2]$. However, for all the numerical examples used in this paper, we have calculated θ using the computational function $\mathtt{atan2}(\sqrt{\mu}, \psi(\mathbf{c}, \mathbf{c}_0))$ which lies in the closed interval $[-\pi, \pi]$. The value of μ is $\geqslant 0$ and if $\psi(\mathbf{c}, \mathbf{c}_0)$ is also positive, which is always the case for the mass with respect to $\mathbf{c}_0$, we have $\theta \geqslant 0$ and it increases when the ratio $\sqrt{\mu}/\psi(\mathbf{c}, \mathbf{c}_0)$ increases. The value of $\psi(\mathbf{c}, \mathbf{c}_0)$ can be negative for the saturation and for the potential and in this case θ continues to be positive because of $\mu \geqslant 0$ and it is decreasing with respect to the absolute value of the ratio. Consequently, even if θ gives an angular value, we can consider the eigenangle as a totally ordered function.

In Fig. 1 for a colour image $\mathbf{f}(\mathbf{x})$ the colour quaternion modulus image $\mathbf{f}^{\rho}(\mathbf{x})$ and eigenangle image $\mathbf{f}^{\theta}(\mathbf{x})$ are compared according to three examples of scalar part.

2.2.2. Quaternion parallel/perpendicular decomposition

It is possible to describe vector decompositions using the product of quaternions. Ell and Sangwine published the following results in [10], which have been recently generalised in [12]. A full quaternion $\mathbf{q}$ may be decomposed about a pure unit quaternion $\mathbf{p}^u$:

$$\mathbf{q} = \mathbf{q}_{\perp} + \mathbf{q}_{\parallel}, \quad (9)$$

the *parallel part* of $\mathbf{q}$ according to $\mathbf{p}^u$, also called the *projection part*, is given by $\mathbf{q}_{\parallel} = S(\mathbf{q}) + V_{\parallel}(\mathbf{q})$, and the *perpendicular part*, also named the *rejection part*, is obtained as $\mathbf{q}_{\perp} = V_{\perp}(\mathbf{q})$ where

$$V_{\parallel}(\mathbf{q}) = \frac{1}{2}(V(\mathbf{q}) - \mathbf{p}^u V(\mathbf{q})\mathbf{p}^u) \quad (10)$$

and

$$V_{\perp}(\mathbf{q}) = \frac{1}{2}(V(\mathbf{q}) + \mathbf{p}^u V(\mathbf{q})\mathbf{p}^u). \quad (11)$$

A diagram illustrating the principle of $\parallel/\perp$ decomposition is depicted in Fig. 2(a).

In the case of colour quaternions, $\mathbf{p}^u$ corresponds to the pure unit quaternion associated to the reference colour $\mathbf{c}_0$, which is defined by

$$\mathbf{q}_0^u = \frac{\hat{r}_0 i + \hat{g}_0 j + \hat{b}_0 k}{\sqrt{\mu_0}} = \hat{r}_{0,u} i + \hat{g}_{0,u} j + \hat{b}_{0,u} k,$$

with $(\hat{r}_{0,u}^2 + \hat{g}_{0,u}^2 + \hat{b}_{0,u}^2) = 1$. By developing the triple product for colour quaternion, it is obtained

Please cite this article in press as: J. Angulo, Geometric algebra colour image representations and derived total orderings for morphological operators – Part I: Colour quaternions, J. Vis. Commun. (2009), doi:10.1016/j.jvcir.2009.10.002

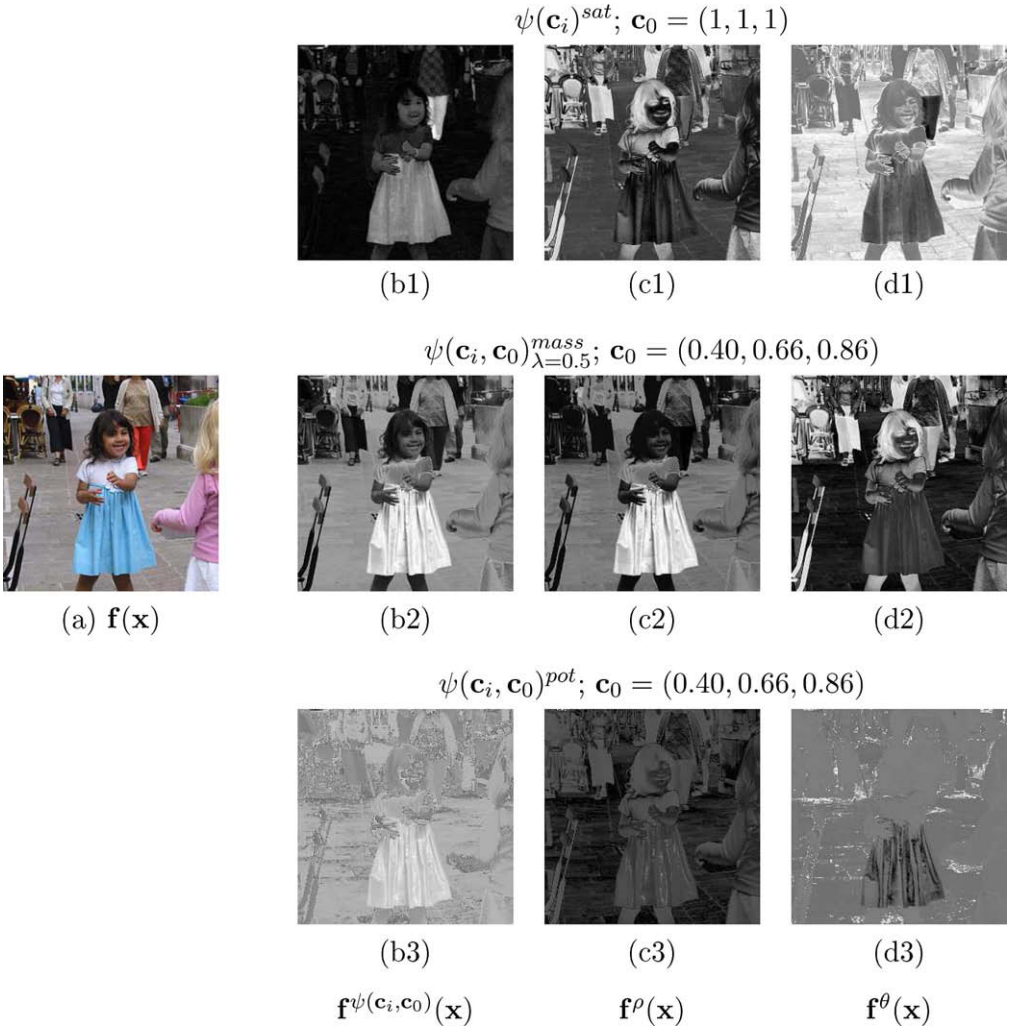

Fig. 1. Colour quaternion modulus image $\mathbf{f}^{\rho}(\mathbf{x})$ (column c) and eigenangle image $\mathbf{f}^{\theta}(\mathbf{x})$ (column d) of the "Carmen" RGB image $\mathbf{f}(\mathbf{x})$ (a) according to three different scalar parts $\mathbf{f}^{\psi(\mathbf{c}_i,\mathbf{c}_0)}(\mathbf{x})$ (column b). Note that images have been normalised to be represented in 8 bits. (For interpretation of color mentioned in this figure the reader is referred to the web version of the article.)

$$\begin{aligned}\mathbf{p}^u V(\mathbf{q})\mathbf{p}^u = &(\hat{r} - 2\hat{r}\hat{r}_{0,u}^2 - 2\hat{g}\hat{r}_{0,u}\hat{g}_{0,u} - 2\hat{b}\hat{r}_{0,u}\hat{b}_{0,u})i \\ &+ (\hat{g} - 2\hat{g}\hat{g}_{0,u}^2 - 2\hat{r}\hat{r}_{0,u}\hat{g}_{0,u} - 2\hat{b}\hat{g}_{0,u}\hat{b}_{0,u})j \\ &+ (\hat{b} - 2\hat{b}\hat{b}_{0,u}^2 - 2\hat{r}\hat{r}_{0,u}\hat{b}_{0,u} - 2\hat{g}\hat{g}_{0,u}\hat{b}_{0,u})k \end{aligned} \quad (12)$$

Now, we can particularize Eqs. (10) and (11) to obtain the following vectorial part and perpendicular part for the unit quaternion $\mathbf{c}_0 = (r_0, r_0, r_0)$ ($\Rightarrow \hat{r}_{0,u} = 1/\sqrt{3}$), which represents the decomposition along the grey axis:

$$V_{\parallel}(\mathbf{q}) = \frac{1}{3}\Big[(\hat{r} + \hat{g} + \hat{b})i + (\hat{r} + \hat{g} + \hat{b})j + (\hat{r} + \hat{g} + \hat{b})k\Big],$$

and

$$V_{\perp}(\mathbf{q}) = \frac{1}{3}\Big[(2\hat{r} - \hat{g} - \hat{b})i + (2\hat{g} - \hat{r} - \hat{b})j + (2\hat{b} - \hat{r} - \hat{g})k\Big].$$

We notice that these projection components correspond respectively to the luminance term and the saturation term, see Rel. (5) and (4). Hence the colour image is decomposed into the intensity information along the grey axis (parallel part) and the chromatic information (perpendicular). Taking another example, for instance $\mathbf{c}_0 = (r_0, r_0/2, 0) (\Rightarrow \hat{r}_{0,u} = \sqrt{\frac{4}{5}})$, we have $V_{\parallel}(\mathbf{q}) = \frac{4}{5}[(\hat{r} + \hat{g}/2)i + (\hat{r}/2 + \hat{g}/4)j]$ and $V_{\perp}(\mathbf{q}) = \frac{4}{5}(\hat{r}/4 - \hat{g}/2)i + \frac{4}{5}(\hat{g} - \hat{r}/2)j + bk$.

Fig. 2 shows also two examples of the decomposition for a colour image. It provides the case $\mathbf{c}_0 = (1,1,1)$ with the intensity information and the chromatic information. The other example corresponds to $\mathbf{c}_0 = (0.75, 0.54, 0.50)$, the typical colour of skin. Considering now the moduli of the decomposed quaternions, i.e.,

$$|\mathbf{q}_{\parallel}| = \sqrt{\psi(\mathbf{c}, \mathbf{c}_0)^2 + |V_{\parallel}(\mathbf{q})|^2}; \quad |\mathbf{q}_{\perp}| = |V_{\perp}(\mathbf{q})|, \quad (13)$$

It should be remarked that the rejection part is a pure quaternion, independent from the scalar part of $\mathbf{q}$, but of course, it depends on the reference colour used for the decomposition. Three examples of the images of the modulus of parallel and perpendicular parts are given in Fig. 3.

3. Total orderings for colour quaternions

We have now all the ingredients to define total orderings between quaternions, $\leqslant_{\Omega^{\mathbf{q}_0^u}}$, and consequently total orderings between associated colours. This objective can be formalised by the following paradigm:

$$\mathbf{q}_i \leqslant_{\Omega^{\mathbf{q}_0^u}} \mathbf{q}_j \Rightarrow \mathbf{c}_i \preccurlyeq \mathbf{c}_j$$

In this context, and using the quaternion representations presented in the previous section, two main families of lexicographical-based partial orderings between colour quaternions can be defined.

Please cite this article in press as: J. Angulo, Geometric algebra colour image representations and derived total orderings for morphological operators – Part I: Colour quaternions, J. Vis. Commun. (2009), doi:10.1016/j.jvcir.2009.10.002

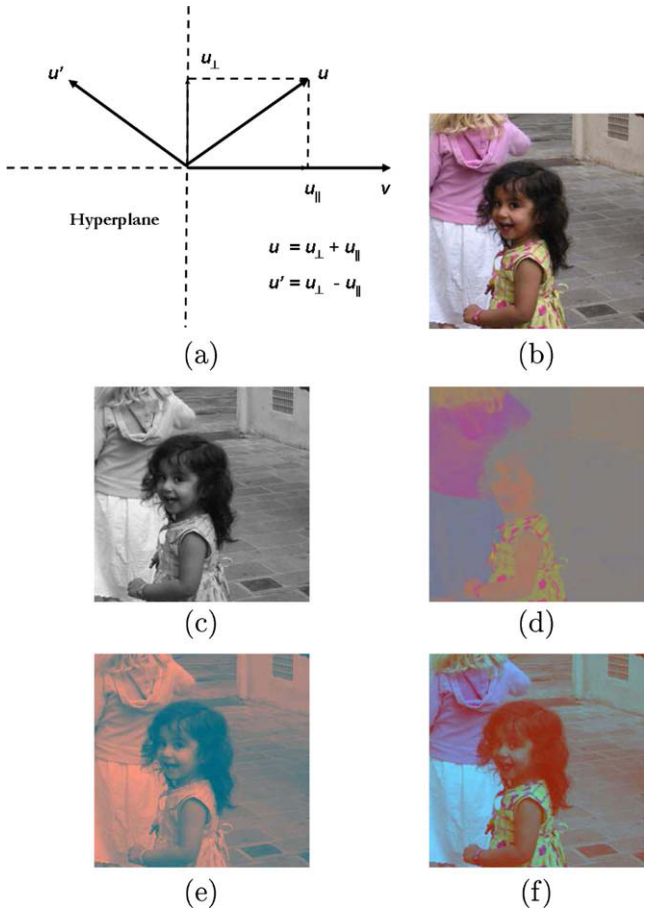

Fig. 2. (a) Decomposition of quaternion $\mathbf{u}$ into its projection and rejection parts according to the unitary quaternion associated to quaternion $\mathbf{v}$. Two examples of colour image decomposition into parallel part and perpendicular part: (b) "Bianca" RGB image $\mathbf{f}(\mathbf{x})$; (c) and (d) respectively, vectorial component of parallel part $\mathbf{f}^{\mathbf{q}}_{\parallel}(\mathbf{x})$ and perpendicular part $\mathbf{f}^{\mathbf{q}}_{\perp}(\mathbf{x})$, where the scalar part of $\mathbf{f}^{\mathbf{q}}(\mathbf{x})$ is $\psi(\mathbf{c}_i,\mathbf{c}_0)^{sat}$ and $\mathbf{c}_0=(1,1,1)$; (e) and (f) respectively, vectorial component of parallel part $\mathbf{f}^{\mathbf{q}}_{\parallel}(\mathbf{x})$ and perpendicular part $\mathbf{f}^{\mathbf{q}}_{\perp}(\mathbf{x})$ where the scalar part of $\mathbf{f}^{\mathbf{q}}(\mathbf{x})$ is $\psi(\mathbf{c}_i,\mathbf{c}_0)^{mass}_{\lambda=0.5}$ and $\mathbf{c}_0=(0.75,0.54,0.50)$. (For interpretation of color mentioned in this figure the reader is referred to the web version of the article.)

3.1. Polar-based orderings

These three approaches are based on ordering according to a priority in the choice of the polar parameters of the quaternion. The ordering $\leqslant_{\Omega_1^{\mathbf{q}_0^u}}$ imposes the priority to the modulus, i.e.,

$$\mathbf{q}_i \leqslant_{\Omega_1^{\mathbf{q}_0^u}} \mathbf{q}_j \iff \begin{cases} \rho_i < \rho_j \text{ or} \\ \rho_i = \rho_j \text{ and } \theta_i < \theta_j \text{ or} \\ \rho_i = \rho_j \text{ and } \theta_i = \theta_j \text{ and } \|\xi_i - \xi_0\| \geqslant \|\xi_j - \xi_0\| \end{cases} \tag{14}$$

where $\|\xi_k - \xi_0\| = \sqrt{(\frac{\hat{r}_k}{\sqrt{\mu_k}} - \frac{\hat{r}_0}{\sqrt{\mu_0}})^2 + (\frac{\hat{g}_k}{\sqrt{\mu_k}} - \frac{\hat{g}_0}{\sqrt{\mu_0}})^2 + (\frac{\hat{b}_k}{\sqrt{\mu_k}} - \frac{\hat{b}_0}{\sqrt{\mu_0}})^2}$ with $\mu_k = \hat{r}_k^2 + \hat{g}_k^2 + \hat{b}_k^2$. In this ordering, for two colour quaternions having the same module the quaternion with bigger eigenangle is bigger or if equals, with the lowest chromatic distance to the reference colour.

Two other orderings can be defined, giving respectively the priority to the value of the eigenangle or to the distance between the eigenaxis and $\mathbf{q}_0^u = \xi_0$, i.e.,

$$\mathbf{q}_i \leqslant_{\Omega_2^{\mathbf{q}_0^u}} \mathbf{q}_j \iff \begin{cases} \theta_i < \theta_j \text{ or} \\ \theta_i = \theta_j \text{ and } \rho_i < \rho_j \text{ or} \\ \theta_i = \theta_j \text{ and } \rho_i = \rho_j \text{ and } \|\xi_i - \xi_0\| \geqslant \|\xi_j - \xi_0\| \end{cases} \tag{15}$$

and

$$\mathbf{q}_i \leqslant_{\Omega_3^{\mathbf{q}_0^u}} \mathbf{q}_j \iff \begin{cases} \|\xi_i - \xi_0\| > \|\xi_j - \xi_0\| \text{ or} \\ \|\xi_i - \xi_0\| = \|\xi_j - \xi_0\| \text{ and } \rho_i < \rho_j \text{ or} \\ \|\xi_i - \xi_0\| = \|\xi_j - \xi_0\| \text{ and } \rho_i = \rho_j \text{ and } \theta_i \leqslant \theta_j \end{cases} \tag{16}$$

However these ones are only partial orderings or pre-orderings, i.e., two distinct colour quaternions, $\mathbf{q}_i \neq \mathbf{q}_j$, can verify the equality of the ordering because even if $\xi_i \neq \xi_j$ their corresponding chromatic distances to the reference can be equal, $\|\xi_i - \xi_0\| = \|\xi_j - \xi_0\|$. In order to have total orderings we propose to complete the proposed cascades with an additional lexicographical cascade of green, then red and finally blue as previously introduced for distance-based orderings [5]; see below for the case of parallel/perpendicular ordering how is completed a pre-ordering.

3.2. Parallel/perpendicular-based ordering

The ordering $\leqslant_{\Omega_4^{\mathbf{q}_0^u}}$ is achieved by considering that a quaternion is bigger than another one with respect to $\mathbf{q}_0^u$ if the modulus of the parallel part is bigger or if the length of parallel parts are equal and the modulus of the perpendicular part is smaller, see the examples depicted in Fig. 4. The schema is only a pre-ordering which is then completed to define the following total ordering:

$$\mathbf{q}_i \leqslant_{\Omega_4^{\mathbf{q}_0^u}} \mathbf{q}_j \iff \begin{cases} |\mathbf{q}_{\parallel i}| < |\mathbf{q}_{\parallel j}| \text{ or} \\ |\mathbf{q}_{\parallel i}| = |\mathbf{q}_{\parallel j}| \text{ and } |\mathbf{q}_{\perp i}| > |\mathbf{q}_{\perp j}| \text{ or} \\ |\mathbf{q}_{\parallel i}| = |\mathbf{q}_{\parallel j}| \text{ and } |\mathbf{q}_{\perp i}| = |\mathbf{q}_{\perp j}| \text{ and} \\ \quad \begin{cases} g_i < g_j \text{ or} \\ g_i = g_j \text{ and } r_i < r_j \text{ or} \\ g_i = g_j \text{ and } r_i = r_j \text{ and } b_i \leqslant b_j \end{cases} \end{cases} \tag{17}$$

Obviously, other orderings are possible by considering a different priority in the choice of the polar and parallel/perpendicular component or even taking the same components but selecting a different sense in the illegalities. For the sake of coherence we limit here our presentation to the above introduced orderings.

3.3. Extremal values

The set of colours in the cube $\mathscr{C}$ is now a totally ordered complete lattice or *chain*. Each ordering relationship introduces a different colour chain and each chain is bounded between the greatest colour $\top^{\Omega^{\mathbf{q}_0^u}}$ (upper bound) and the least colour $\bot^{\Omega^{\mathbf{q}_0^u}}$ (lower bound). The extremal values of each colour chain are very important to understand the effect of the corresponding colour dilation and erosion.

The bounds of each quaternionic ordering depend obviously on the type of scalar part. We should consider separately the three type of proposed $\psi(\mathbf{c}_i,\mathbf{c}_0)$ to calculate the greatest and least colours of each $\Omega^{\mathbf{q}_0^u}$. For the sake of simplicity, we limit here our presentation to the case of the saturation as scalar part since the analysis for the mass or the potential depends strongly on the reference colour.

Let us consider that $\rho^{sat} = \sqrt{\psi^2 + \mu}$ and $\theta^{sat} = \arctan(\sqrt{\mu}/\psi)$, where $\psi = (s - 0.5)$ and $\mu = (r-0.5)^2 + (g-0.5)^2 + (b-0.5)^2$. The saturation equals 0 when $r = g = b (\psi = -0.5)$ and consequently $\psi^2 = 0.25$. Note that $\psi^2 = 0.25$ also when saturation is maximal ($s = 1 \Rightarrow \psi = 0.5$), which is the case for all six dominant

Please cite this article in press as: J. Angulo, Geometric algebra colour image representations and derived total orderings for morphological operators – Part I: Colour quaternions, J. Vis. Commun. (2009), doi:10.1016/j.jvcir.2009.10.002

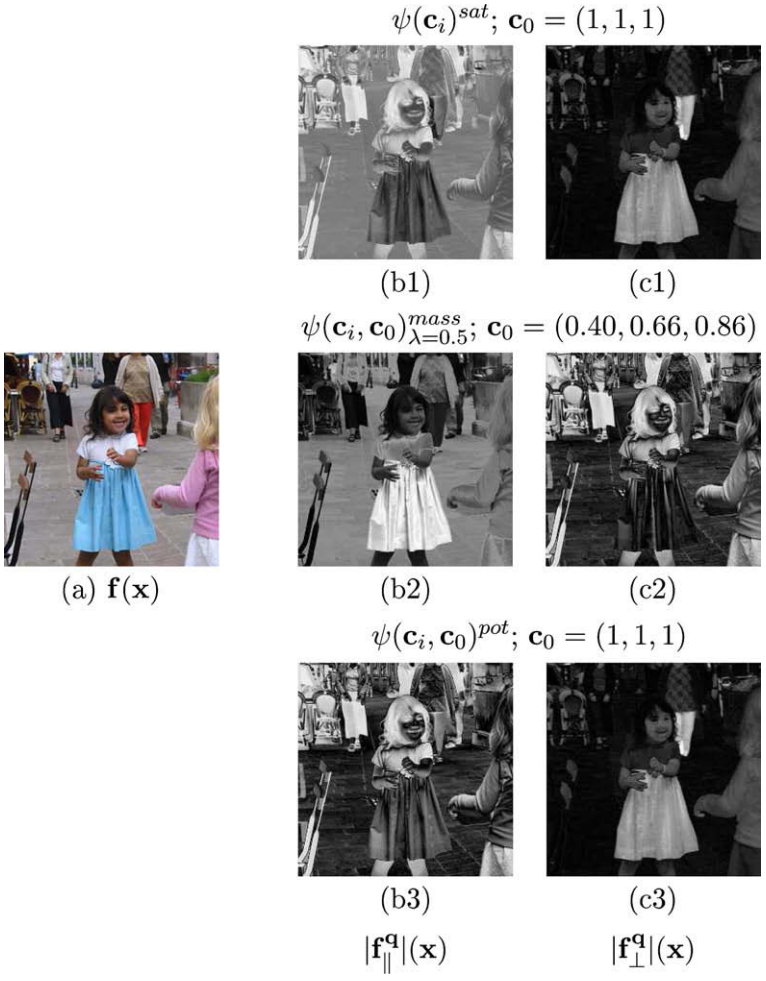

Fig. 3. Colour quaternion decomposition about the unit quaternion associated to reference colour $\mathbf{c}_0$: image of modulus of parallel part $|\mathbf{f}^{\mathbf{q}}_{\parallel}|(\mathbf{x})$ (column b) and image of modulus of perpendicular part $|\mathbf{f}^{\mathbf{q}}_{\perp}|(\mathbf{x})$ (column c) of "Carmen" RGB image $\mathbf{f}(\mathbf{x})$ (a) according to three different scalar parts. (For interpretation of color mentioned in this figure the reader is referred to the web version of the article.)

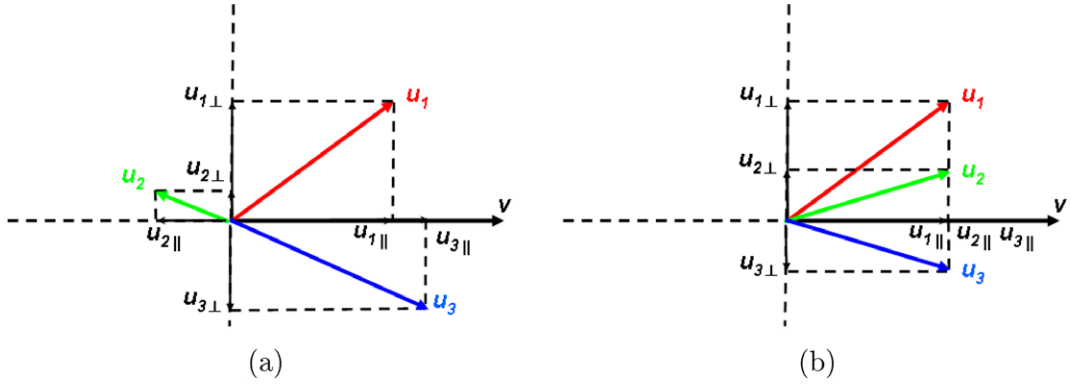

Fig. 4. Ordering of quaternions $\mathbf{u}_i$ according to their decomposition $\mathbf{u}_{i\parallel} + \mathbf{u}_{i\perp}$ about the pure quaternion $\mathbf{v}$: (a) $|\mathbf{u}_{3\parallel}| > |\mathbf{u}_{1\parallel}| > |\mathbf{u}_{2\parallel}| \Rightarrow \mathbf{u}_3 > \mathbf{u}_1 > \mathbf{u}_2$ and (b) $|\mathbf{u}_{1\parallel}| = |\mathbf{u}_{2\parallel}|$ and $|\mathbf{u}_{1\perp}| > |\mathbf{u}_{2\perp}| \Rightarrow \mathbf{u}_1 < \mathbf{u}_2$. But quaternions $\mathbf{u}_2$ and $\mathbf{u}_3$ which have equal modulus of both parallel and perpendicular parts cannot be ordered without an additional condition.

chromatic colours, i.e., colours defined only by ones and zeros. It is obtained for these six dominant chromatic colours and for $\mathbf{c} = (0,0,0)$ and $\mathbf{c} = (1,1,1)$ that $\mu = 0.75$ and the corresponding value $\rho^{sat} = 1$. It is easy to verify that $\psi^2 = 0$ when $s = 0.5$, which corresponds to colours including the three values 0.25, 0.50 and 0.75, e.g., $\mathbf{c} = (0.25, 0.75, 0.50)$. These points have $\mu = 0.125$ and then $\rho^{sat} = 0.35$. The minimum $\mu = 0$ is obtained only for the center of the cube, $\mathbf{c} = (0.5, 0.5, 0.5)$, which involves $\rho^{sat} = 0.5$. Consequently, we have the following interval of variation: $0.35 \leqslant \rho^{sat} \leqslant 1$. Using for θ^{sat} the function `atan2`, we obtain the max bound $\theta^{sat} = \pi$ when $\mu = 0$ which is the case for $\mathbf{c} = (0.5, 0.5, 0.5)$, independently of the value of ψ. If $\mu = 0.75$ and $\psi = -0.5$ the obtained value is $\theta^{sat} = 2.09$, and with $\mu = 0.75$ and $\psi = 0.5$ we get $\theta^{sat} = 1.04$. This last value is the min bound for θ^{sat}. Hence $1.04 \leqslant \theta^{sat} \leqslant \pi$. The bounds for the chromatic distance are independent of the scalar part but depend strongly on the

Please cite this article in press as: J. Angulo, Geometric algebra colour image representations and derived total orderings for morphological operators – Part I: Colour quaternions, J. Vis. Commun. (2009), doi:10.1016/j.jvcir.2009.10.002

reference colour. More precisely, $0 \leqslant \|\boldsymbol{\xi} - \boldsymbol{\xi}_0\| \leqslant D$, where $D = 2.31$ is the distance between $\mathbf{c} = (0,0,0)$ and $\mathbf{c}_0 = (1,1,1)$ (or vice versa). For any particular colour chain, the chromatic distance equals 0 for any colour having the same chromaticity than centered $\mathbf{c}_0$. The maximal distance corresponds to one of the main colour points, e.g., for $\mathbf{c}_0 = (0.2, 0.2, 0.5)$ the max distance is for the colour point $(1,1,0)$. The interval of definition of the modulus for both $\|$ and $\perp$ components depends also on the choice of the reference colour. In addition, it should be reminded that the modulus of the parallel part relies also on the scalar part. For instance, if $\mathbf{c}_0 = (1,1,1)$, the $|\mathbf{q}_\perp| = |V_\perp(\mathbf{q})|$ is the saturation of centered colours in norm L_2, which is max with value $|\mathbf{q}_\perp| = 0.4$ for the six chromatic colours and the min $|\mathbf{q}_\perp| = 0$ for all the colours in the chromatic axis, i.e., $r = g = b$. The value of $|V_\parallel(\mathbf{q})|$ is 0 for the center of the cube $\mathbf{c}_0 = (0.5, 0.5, 0.5)$ and the max $|V_\parallel(\mathbf{q})| = 0.86$ is obtained for the extremes of the grey axis. For other colour references, the corresponding extremes for $|\mathbf{q}_\perp|$ and $|\mathbf{q}_\parallel|$ can be also computed in such a way.

After this numerical analysis, we can now summarise as follows the extremes of the quaternionic orderings for the saturation as scalar part:

- $\top_{sat}^{\Omega_1^{\mathbf{q}_0^u}} \equiv (1,1,1)$ or $(0,0,0)$ depending on which one is the closest to the reference colour $\mathbf{c}_0$,
- $\perp_{sat}^{\Omega_1^{\mathbf{q}_0^u}} \equiv$ The intermediate achromatic colour (including the three values 0.25, 0.5 and 0.75) farthest from the reference colour $\mathbf{c}_0$,
- $\top_{sat}^{\Omega_2^{\mathbf{q}_0^u}} \equiv (0.5, 0.5, 0.5)$,
- $\perp_{sat}^{\Omega_2^{\mathbf{q}_0^u}} \equiv$ The farthest dominant chromatic colour from the reference colour $\mathbf{c}_0$,
- $\top_{sat}^{\Omega_3^{\mathbf{q}_0^u}} \equiv$ The closest colour to the reference colour $\mathbf{c}_0$ having maximal ρ^{sat},
- $\perp_{sat}^{\Omega_3^{\mathbf{q}_0^u}} \equiv$ The farthest dominant colour (six chromatic ones+white/black) from the reference colour $\mathbf{c}_0$,
- $\top_{sat}^{\Omega_4^{\mathbf{q}_0^u}}, \mathbf{c}_0 = (1,1,1) \equiv (1,1,1)$,
- $\perp_{sat}^{\Omega_4^{\mathbf{q}_0^u}}, \mathbf{c}_0 = (1,1,1) \equiv$ The intermediate achromatic colour (including the three values 0.25, 0.5 and 0.75) farthest from the reference colour $\mathbf{c}_0$.

There is another important notion to interpret the effects of sup and inf operators in a colour chain. Given to colours $\mathbf{c}_i$ and $\mathbf{c}_j$, we say that $\mathbf{c}_i$ is *closer to* $\top^{\Omega^{\mathbf{q}_0^u}}$ than $\mathbf{c}_j$ if $\mathbf{c}_j \leqslant_{\Omega^{\mathbf{q}_0^u}} \mathbf{c}_i \leqslant_{\Omega^{\mathbf{q}_0^u}} \top^{\Omega^{\mathbf{q}_0^u}}$. Consequently, in a subset of colours, the closest colour to $\top^{\Omega^{\mathbf{q}_0^u}}$ is the biggest one and the farthest is the smallest one. In a discrete colour chain, such as the case for the digital colour images, we can also define the *distance in the chain of two colours* $\mathbf{c}_i$ and $\mathbf{c}_j$ as the number of intermediate colours between them. Then, we can calculate for each colour its distance to $\top^{\Omega^{\mathbf{q}_0^u}}$ and to $\perp^{\Omega^{\mathbf{q}_0^u}}$.

3.4. Invariance properties of orderings

Let $\mathscr{T}$ and $\mathscr{T}\prime$ be two ordered set of grey-levels, i.e., two complete lattices. Consider the mapping $A : \mathscr{T} \to \mathscr{T}'$, then we say that an ordering $\leqslant_\Omega$ is invariant under A (or respected by A) if

$$x \leqslant_\Omega y \Longleftrightarrow A(x) \leqslant_\Omega A(y) \quad \forall x, y \in \mathscr{T}. \tag{18}$$

As we can suppose, it may or may not be possible to fund such an invariant ordering, depending on the nature of the A. The concepts of ordering invariance and of commutation of sup and inf operators under intensity image transformations have been well studied in the theory of complete lattices [37,27]. More precisely, in mathematical morphology a mapping $A : \mathscr{T} \to \mathscr{T}'$ which satisfies the criterion (18) is called an *anamorphosis*. It is well known for the grey-tone case that any strictly increasing mapping A is an anamorphosis. Theoretical results on anamorphoses for multivalued lattice such as colour images were studied by Serra [38].

We are interested here to study the behaviour of quaternionic total ordering with respect to digital colour image transformations having a physical sense. In particular, for any grey level value $p_i \in \mathscr{T}$, there are two typical mappings used in many devices and imaging software:

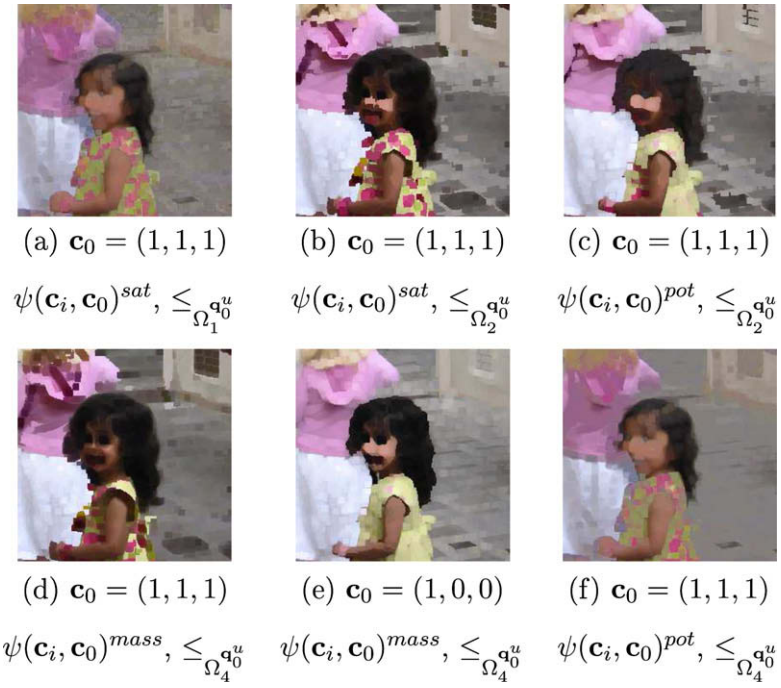

Fig. 5. Comparative of colour erosions $\varepsilon_{\Omega,nB}(\mathbf{f})(\mathbf{x})$ (the structuring element B is a disk and the size is $n = 7$) on image "Bianca" using different quaternionic orderings and with different scalar parts. (For interpretation of color mentioned in this figure the reader is referred to the web version of the article.)

Please cite this article in press as: J. Angulo, Geometric algebra colour image representations and derived total orderings for morphological operators – Part I: Colour quaternions, J. Vis. Commun. (2009), doi:10.1016/j.jvcir.2009.10.002

- Linear transformation: $A_1(p_i) = \alpha p_i + \beta$, with $\alpha > 0$ and $\beta \in \mathbb{R}$.
- Gamma correction: $A_2(p_i) = p_i^{\gamma}$, with $\gamma > 0$. To make calculations easier, we can take the limited expansion of first order as linear approximation, for p_i near to 1, and consider the following correction function $A_2(p_i) \cong \gamma p_i + (1-\gamma)$.

Both transformations are clearly anamorphosis for grey-images. Let us consider now a family of three independent anamorphosis $\mathbf{A} = (A_R, A_G, A_B)$ for each R, G and B colour components. The mapping $\mathbf{A}$ does not generate always a product anamorphosis from $\mathscr{T}^{rgb}$ onto $\mathscr{T}^{rgb'}$. It will depend on the total ordering $\leqslant_\Omega$ of the complete lattice $\mathscr{T}^{rgb}$. In our case, we focus on uniform colour mappings, that is the same transformation is applied to each colour component, i.e., $A_R = A_G = A_B = A$. A counterexample, out of the scope of our analysis, is the white balance transformation which involves a different linear transformation for each colour component.

By the way, our problem here is more tricky. A colour $\mathbf{c}_i$ is transformed into another different colour $\mathbf{c}'_i = \mathbf{A}(\mathbf{c}_i) = (A(r_i), A(g_i), A(b_i)) = (r'_i, g'_i, b'_i)$, but what is the corresponding transformed colour quaternion $\mathbf{q}'_i = \mathbf{Q}(\mathbf{q}_i)$? Obviously the mapping $\mathbf{Q}$ will depend on the scalar part. Furthermore, the quaternionic colour orderings are not based directly on the four quaternion components derived from transformation $\mathbf{Q}$ but on the variables of quaternion decompositions. In conclusion, we need to check if the RGB linear anamorphosis involves also anamorphosis in the transformed quaternionic polar and parallel/perpendicular representations, and of course, the reference colour $\mathbf{c}_0$ is kept constant.

In order to take into account the centering of colours, let us start by rewriting $c'_i = A_1(c_i) = \alpha c_i + \hat{\beta}$ with $\hat{\beta} = \beta - 0.5$ for the transformation each colour component r_i, g_i and b_i of colour i. It is easy to check that $\psi(\mathbf{c}'_i, \mathbf{c}_0)^{sat} = \alpha\psi(\mathbf{c}_i, \mathbf{c}_0)^{sat}$. The mass and the potential with respect to $\mathbf{c}_0$ depends on distances. For the Euclidean distance, we have $\|\mathbf{c}'_i - \mathbf{c}_0\|_2^2 = \|\alpha\mathbf{c}_i - \mathbf{c}_0\|_2^2 + 2\alpha\hat{\beta}\|\mathbf{c}_i\|_1 - \hat{\beta}\|\mathbf{c}_0\|_1 + 3\hat{\beta}^2$. Consequently $\|\mathbf{c}'_i - \mathbf{c}_0\|_2 \leqslant \|\mathbf{c}'_j - \mathbf{c}_0\|_2 \Longleftrightarrow \|\mathbf{c}_i - \mathbf{c}_0\|_2 \leqslant \|\mathbf{c}_j - \mathbf{c}_0\|_2$ iff $\hat{\beta} = 0$ or $\|\mathbf{c}_i\|_1 = \|\mathbf{c}_j\|_1$. The last condition is achieved by normalising the colour components, i.e., normalised red is $\tilde{r}_i = r_i/(r_i + g_i + b_i)$, with identical calculation for the two other components, and consequently $\|\tilde{\mathbf{c}}_i\|_1 = \|\tilde{\mathbf{c}}_j\|_1 = 1$. This kind of normalisation against intensity variations is well known in colour invariance, see for instance Gevers and Smeulders [15]. The invariance of the angle between the transformed colours and $\mathbf{c}_0$, which corresponds to the chromatic distance, needs very specific conditions. Hence we propose to set up $\lambda = 1$ for the mass, and then, the conditions derived from the Euclidean distance make the transformed mass $\psi(\mathbf{c}'_i, \mathbf{c}_0)_{\lambda=1}^{mass}$ and potential $\psi(\mathbf{c}'_i, \mathbf{c}_0)^{pot}$ ordering invariant.

The first variable used in the quaternion polar decomposition is the modulus: $\rho'_i = \sqrt{\psi(\mathbf{c}'_i, \mathbf{c}_0)^2 + \mu'_i}$, where $\mu_i = \|\mathbf{c}_0\|_2^2$ and $\mu'_i = \alpha^2\|\mathbf{c}_0\|_2^2 + 2\alpha\hat{\beta}\|\mathbf{c}_0\|_1 + 3\hat{\beta}^2$. According to the previous analysis, we have justified the ordering preservation of scalar parts, and consequently of the squared counterparts. We need to verify if $\rho'_i \leqslant \rho'_j \Longleftrightarrow \rho_i \leqslant \rho_j$, or more precisely, under which conditions $\mu'_i \leqslant \mu'_j \Longleftrightarrow \mu_i \leqslant \mu_i$. The equivalence of norms guarantees that $\|\mathbf{c}_i\|_1 \leqslant \|\mathbf{c}_j\|_1 \Longleftrightarrow \|\mathbf{c}_i\|_2 \leqslant \|\mathbf{c}_j\|_2$, so again the same conditions of no translation or L_1 normalised colours is a sufficient condition. In the case of the eigenangle $\theta'_i = \arctan(\sqrt{\mu'_i}/\psi(\mathbf{c}'_i, \mathbf{c}_0))$, a similar analysis shows that only $\hat{\beta} = 0$ guarantees ordering invariance. And this is also the case for the invariance of $\|\xi'_i - \xi_0\| \leqslant \|\xi'_j - \xi_0\|$.

Concerning the parallel/perpendicular decomposition, we can also easily calculate the modulus of the decomposed transformed quaternions. Their simplified expressions are

$$|V_{\parallel}(\mathbf{q}'_i)|^2 = \alpha^2 \frac{\langle \mathbf{c}_i, \mathbf{c}_0\rangle^2}{\|\mathbf{c}_0\|_2^2} + 2\alpha\hat{\beta}\frac{\|\mathbf{c}_0\|_1}{\|\mathbf{c}_0\|_2^2}\langle \mathbf{c}_i, \mathbf{c}_0\rangle + \hat{\beta}^2\frac{\|\mathbf{c}_0\|_1^2}{\|\mathbf{c}_0\|_2^2},$$

and

$$|V_{\perp}(\mathbf{q}'_i)|^2 = \alpha^2\left(\|\mathbf{c}_0\|_2^2 - \frac{\langle \mathbf{c}_i, \mathbf{c}_0\rangle^2}{\|\mathbf{c}_0\|_2^2}\right) + 2\alpha\hat{\beta}\left(\|\mathbf{c}_i\|_1 - \frac{\|\mathbf{c}_0\|_1}{\|\mathbf{c}_0\|_2^2}\langle \mathbf{c}_i, \mathbf{c}_0\rangle\right) + 2\hat{\beta}^2\left(1 - \frac{r_0g_0 + r_0b_0 + g_0b_0}{\|\mathbf{c}_0\|_2^2}\right).$$

The terms of $\hat{\beta}^2$ depends only on $\mathbf{c}_0$ and the term of α^2 corresponds to the original values $|V_{\parallel}(\mathbf{q})|^2$ and $|V_{\perp}(\mathbf{q})|^2$. Due to the fact that r, g and b are positive, one has $\langle \mathbf{c}, \mathbf{c}_0\rangle \geqslant 0$ and as it was imposed that $\alpha > 0$, we have that $|V_{\parallel}(\mathbf{q}'_i)| \leqslant |V_{\parallel}(\mathbf{q}'_j)| \Longleftrightarrow |V_{\parallel}(\mathbf{q}_i)| \leqslant |V_{\parallel}(\mathbf{q}_j)|$ iff $\hat{\beta} \geqslant 0$. A similar analysis leads to the same condition which guarantees also that $|V_{\perp}(\mathbf{q}'_i)| \leqslant |V_{\perp}(\mathbf{q}'_j)| \Longleftrightarrow |V_{\perp}(\mathbf{q}_i)| \leqslant |V_{\perp}(\mathbf{q}_j)|$.

To conclude, we can assert that only under strict conditions the colour quaternionic orderings are invariant to RGB uniform linear colour transformations. In the forthcoming second part of this paper on colour morphology using tensor representations, the search of invariant orderings is a strong motivation in the definition of derived tensor orderings.

Another theoretical point to be considered in future work is the duality of colour operators with respect to the complementation of colours (i.e., negative of colour components). In practice, this useful property allows us in mathematical morphology to implement exclusively the dilation, and using the complement, to be able to obtain the corresponding erosion. Quaternion duality implies the notion of quaternion involutions which have been recently formalised by Ell and Sangwine [12].

3.5. Comparison with classical colour total orderings

The presented lexicographical four orderings are conceptually different from the previous colour total orderings proposed in the literature. However, a comparison with previous works allows us to identify some common characteristics.

In [2], an ordering based on giving the priority to a linear combination of luminance and saturation was used to build colour levellings. At a first look, this seems similar to the ordering $\leqslant_{\Omega_0^{\mathbf{q}''}}$, using saturation as scalar part. However, as pointed above, in this particular case the module is a combination of saturation and a RGB energy associated to the distance from the mid-grey and not directly to an intensity of energy in the sense of luminance.

In previous works many attention has been paid to define total orderings adapted to the hue, considered as an angular component defined in the unit circle [20,19]. We remark again that the angular component θ can be considered as an ordered function without the need to define an origin of angles. This last condition is required for defining a total ordering in the hue component.

The ordering $\leqslant_{\Omega_0^{\mathbf{q}''}}$, based on giving priority to the chromatic distance between each colour and the colour of reference, is fundamentally a distance-based ordering which corresponds to the framework studied previously in detail in [5]. No major interest is found to this kind of ordering to consider the colour as a full quaternion. This is just the reason why this ordering has not been evaluated in the empirical part of this study. This type of ordering is very useful for colour filtering and the reader interested in more details can consult the paper [5].

Finally, orderings based on projecting the colour along a reference colour, and in particular the projection with respect to the grey axis, were studied in [16] to construct exclusively colour levellings (see below the definition of levelling operator). The projection principle is quite similar to the ordering $\leqslant_{\Omega_0^{\mathbf{q}''}}$, but note that here we are decomposing full quaternions with a scalar part. We notice that if $\psi(\mathbf{c}_i, \mathbf{c}_0) = 0$ the moduli of $\|/\perp$ decompositions about $\mathbf{c}_0 = (1,1,1)$ yields to the luminance and saturation.

Please cite this article in press as: J. Angulo, Geometric algebra colour image representations and derived total orderings for morphological operators – Part I: Colour quaternions, J. Vis. Commun. (2009), doi:10.1016/j.jvcir.2009.10.002

Mathematical morphology operators based on lexicographical orderings for luminance and saturation components have been widely studied in the literature [19,3]. However, contrary to the order $\leqslant_{\Omega_4^{\mathbf{q}_0^u}}$, with $\psi(\mathbf{c}_i,(1,1,1))=0$, all the proposed previous approaches consider luminance and saturation in the same sense (i.e., bright chromatic colours are bigger than bright achromatic ones) whereas here we give priority to bright/dark achromatic colours.

In summary, the quaternionic representations involve a rich framework which, on the one hand, generalises many of the previously studied total orderings for colour images; and on the other hand, introduces new total orderings based on geometric decompositions tailored by a reference colour.

4. Colour quaternionic mathematical morphology

Once the family of quaternionic total orderings $\leqslant_\Omega$ has been established, the morphological colour operators are defined in the standard way. We limit here our developments to the flat operators, i.e., the structuring elements are planar. The non planar structuring functions are defined by weighting values on their support [37]. The implementation and the use of colour structuring functions will be the object of future research.

We need to recall a few notions which characterise the properties of morphological operators. Let ψ be an operator on a complete lattice $\mathcal{F}(E,\mathcal{T}^{rgb})$. ψ is increasing if $\forall \mathbf{f},\mathbf{g}\in\mathcal{F}(E,\mathcal{T}^{rgb}), \mathbf{f}\leqslant_\Omega\mathbf{g} \Rightarrow \psi(\mathbf{f})\leqslant_\Omega\psi(\mathbf{f})$. It is anti-extensive if $\psi_\Omega(\mathbf{f})\leqslant_\Omega\mathbf{f}$ and it is extensive if $\mathbf{f}\leqslant_\Omega\psi_\Omega(\mathbf{f})$. An operator is idempotent if it is verified that $\psi(\psi(\mathbf{f}))=\psi(\mathbf{f})$.

4.1. Erosion and dilation

The *colour erosion* of an image $\mathbf{f}\in\mathcal{F}(E,\mathcal{T}^{rgb})$ at pixel $\mathbf{x}\in E$ by the structuring element $B\subset E$ of size n is given by

$$\varepsilon_{\Omega,nB}(\mathbf{f})(\mathbf{x})=\{\mathbf{f}(\mathbf{y}):\mathbf{f}(\mathbf{y})=\wedge_\Omega[\mathbf{f}(\mathbf{z})],\mathbf{z}\in n(B_\mathbf{x})\}, \tag{19}$$

where $\inf_\Omega$ is the infimum according to the total ordering $\leqslant_\Omega$. The corresponding *colour dilation* $\delta_{\Omega,nB}$ is obtained by replacing the $\inf_\Omega$ by the $\sup_\Omega$, i.e.,

$$\delta_{\Omega,nB}(\mathbf{f})(\mathbf{x})=\{\mathbf{f}(\mathbf{y}):\mathbf{f}(\mathbf{y})=\vee_\Omega[\mathbf{f}(\mathbf{z})],\mathbf{z}\in n(B_\mathbf{x})\}. \tag{20}$$

Erosion and dilation are increasing operators. Moreover, erosion is anti-extensive and dilation is extensive. In practice, the colour erosion shrinks the structures which have a colour close to $\top^\Omega$; "peaks of colour" thinner than the structuring element disappear by taking the colour of neighboring structures with a colour away

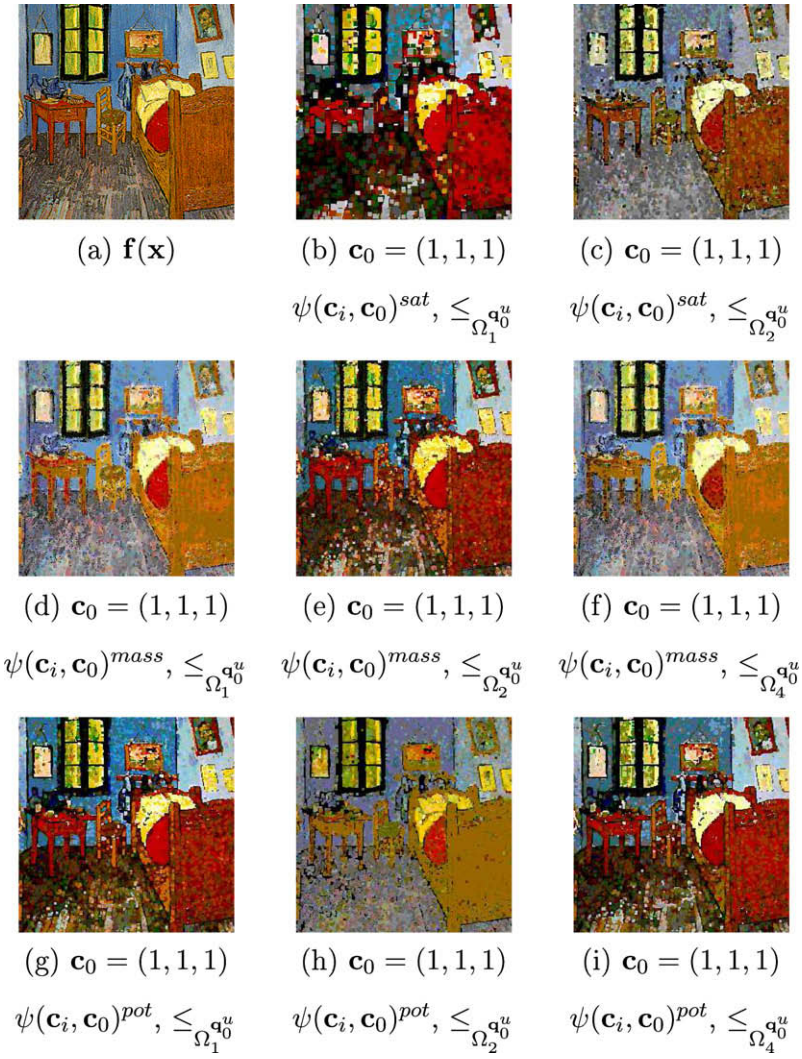

Fig. 6. Comparative of colour closings $\varphi_{\Omega,nB}(\mathbf{f})(\mathbf{x})$ (the structuring element B is a disk and the size is $n=5$) on image "Bedroom in Arles" (detail of painting by Van Gogh) using different quaternionic orderings and with different scalar parts. (For interpretation of color mentioned in this figure the reader is referred to the web version of the article.)

Please cite this article in press as: J. Angulo, Geometric algebra colour image representations and derived total orderings for morphological operators – Part I: Colour quaternions, J. Vis. Commun. (2009), doi:10.1016/j.jvcir.2009.10.002

from $\top^{\Omega}$. As well, it expands the structures which have a colour close to $\perp_{\Omega}$. Dilation produces the dual effects, enlarging the regions having a colour close to $\perp_{\Omega}$ and contracting the others.

4.2. Morphological filters

In general, a morphological filter is an increasing operator that is also idempotent (erosion/dilation are not idempotent).

4.2.1. Opening and closing

A *colour opening* is an erosion followed by a dilation, i.e.,

$$\gamma_{\Omega,nB}(\mathbf{f}) = \delta_{\Omega,nB}(\varepsilon_{\Omega,nB}(\mathbf{f})), \tag{21}$$

and a *colour closing* is a dilation followed by an erosion, i.e.,

$$\varphi_{\Omega,nB}(\mathbf{f}) = \varepsilon_{\Omega,nB}(\delta_{\Omega,nB}(\mathbf{f})). \tag{22}$$

The opening (closing) is an anti-extensive (extensive) operator. More precisely, the opening removes colour peaks that are thinner than the structuring element, having a colour close to $\top^{\Omega}$; the closing removes colour peaks that are thinner than the structuring element, having a colour far from $\top^{\Omega}$, i.e., close to $\perp^{\Omega}$.

4.2.2. Alternate sequential filters

Once the colour opening and closing are defined it is indubitable how to extend other classical operators such as the *colour alternate sequential filters* (or ASF), obtained by concatenation of openings and closings, i.e.,

$$ASF(\mathbf{f})_{\Omega,nB} = \varphi_{\Omega,nB}\gamma_{\Omega,nB}\cdots\varphi_{\Omega,2B}\gamma_{\Omega,2B}\varphi_{\Omega,B}\gamma_{\Omega,B}(\mathbf{f}). \tag{23}$$

A dual family of ASF operators is obtained by changing the order of the openings/closings. The ASF act simultaneously on the peaks and the valleys, simplifying (smoothing) them. They are useful when dealing with noisy signals.

4.2.3. Residue-based operators

Moreover, using a colour metric to calculate the image distance d, $d \in \mathscr{F}(E,\mathscr{T})$ (a scalar function), given by the difference point-by-point of two colour images $d(\mathbf{x}) = \|\mathbf{f}(\mathbf{x}) - \mathbf{g}(\mathbf{x})\|$, we can easily define the *morphological colour gradient*, i.e.,

$$\varrho_{\Omega}(\mathbf{f}) = \|\delta_{\Omega,B}(\mathbf{f}) - \varepsilon_{\Omega,B}(\mathbf{f})\|. \tag{24}$$

This function gives the contours of the image, attributing more importance to the transitions between regions close/far to the extremes $\top^{\Omega}$ and $\perp^{\Omega}$. The *positive colour top-hat transformation* is the residue of a colour opening, i.e.,

$$\rho^{+}_{\Omega,nB}(\mathbf{f}) = \|\mathbf{f} - \gamma_{\Omega,nB}(\mathbf{f})\|. \tag{25}$$

Dually, the *negative colour top-hat transformation* is given by

$$\rho^{-}_{\Omega,nB}(\mathbf{f}) = \|\varphi_{\Omega,nB}(\mathbf{f}) - \mathbf{f}\|. \tag{26}$$

The top-hat transformation yields greylevel images and is used to extract contrasted components with respect to the background, where the background corresponds to the structures of colour

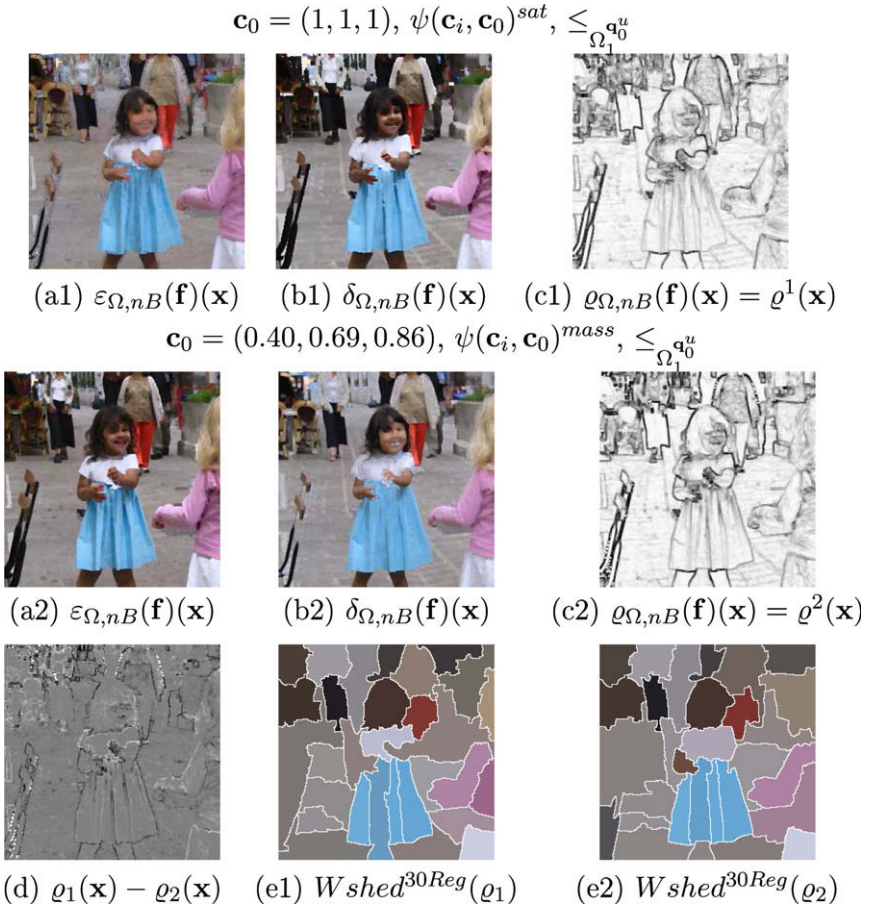

Fig. 7. Comparative of two colour morphological gradients on image "Carmen": considering the same ordering $\leqslant_{\Omega_1^{\mathbf{q}_0^u}}$, and changing the scalar component, with the saturation and the mass (using as reference $\mathbf{c}_0$ the blue colour of the skirt). In the last row, the image (d) gives the difference between both gradients (in white, pixels where $\varrho_1(x)$ is bigger than $\varrho_2(x)$ and in black, the dual case). The images (e1) and (e2) correspond to the segmentation by hierarchical watershed in 30 regions of gradient $\varrho_1(x)$ and $\varrho_2(x)$, respectively. (For interpretation of color mentioned in this figure the reader is referred to the web version of the article.)

Please cite this article in press as: J. Angulo, Geometric algebra colour image representations and derived total orderings for morphological operators – Part I: Colour quaternions, J. Vis. Commun. (2009), doi:10.1016/j.jvcir.2009.10.002

close to $\perp^{\Omega}$ for $\rho^{+}_{\Omega,nB}$ and close to $\top^{\Omega}$ for $\rho^{-}_{\Omega,nB}$. Moreover, top-hats remove the slow trends, and thus enhances the contrast of objects smaller than the structuring element used for the opening/closing.

4.2.4. Geodesic reconstruction and derived operators

In addition, we also propose the extension of operators "by reconstruction", implemented by means of the geodesic dilation. The *colour geodesic dilation* is based on restricting the iterative dilation of a function marker $\mathbf{m}$ by B to a function reference $\mathbf{f}$ [44], i.e.,

$$\delta^{n}_{\Omega}(\mathbf{m},\mathbf{f}) = \delta^{1}_{\Omega}\delta^{n-1}_{\Omega}(\mathbf{m},\mathbf{f}), \tag{27}$$

where the unitary conditional dilation is given by $\delta^{1}_{\Omega}(\mathbf{m},\mathbf{f}) = \delta_{\Omega,B}(\mathbf{m}) \wedge_{\Omega} \mathbf{f}$. Typically, B is an isotropic structuring element of size 1.

The *colour reconstruction* by dilation is then defined by

$$\gamma^{rec}_{\Omega}(\mathbf{m},\mathbf{f}) = \delta^{i}_{\Omega}(\mathbf{m},\mathbf{f}), \tag{28}$$

such that $\delta^{i}_{\Omega}(\mathbf{m},\mathbf{f}) = \delta^{i+1}_{\Omega}(\mathbf{m},\mathbf{f})$ (idempotence). Whereas the adjunction opening $\gamma_{\Omega,nB}(\mathbf{f})$ (from an erosion/dilation) modifies the colour contours, the associated opening by reconstruction $\gamma^{rec}_{\Omega}(\mathbf{m},\mathbf{f})$ (where the marker is $\mathbf{m} = \varepsilon_{\Omega,nB}(\mathbf{f})$ or $\mathbf{m} = \gamma_{\Omega,nB}(\mathbf{f})$) is aimed at efficiently and precisely reconstructing the contours of the colour objects having a colour close to $\top^{\Omega}$ and which have not been totally removed by the marker filtering process.

5. Results and discussion

We explore in this section the effects of these morphological operators when they are applied to colour images according to the family of quaternionic total orderings introduced in this paper. We try to illustrate a wide variety of morphological colour operators by analysing the choices of the scalar part and of reference colour in the various orderings. Even if we are conscious that a further study would need more extensive comparisons, we consider that the following comparative examples allow us to draw some interesting conclusions. In addition, in the last part of this section, we focus on a particular application domain, the image-based traffic applications, to show the usefulness of the proposed operators for real life complex problems.

In Fig. 5 a comparative of erosions using different quaternionic orderings is given, with different scalar parts. The same structuring element, i.e., the same "shape and size of operation", has been applied in the six cases. As we can observe from the examples, the effects of the various orderings are quite different. For instance, $\leqslant_{\Omega_0^{\mathbf{q}_u}}$ (Fig. 5(a)), with saturation as scalar part, enlarges regions of achromatic middle intensity colours (i.e., close to $\perp^{\Omega_1^{\mathbf{q}_0}}$) and reduces the zones of achromatic and chromatic ones situated close to the extreme parts of the RGB cube. The other results can be interpreted with the help of the analysis of orderings discussed in previous sections. We notice also the influence of the choice of the reference colour when, for instance, the mass is taken as scalar part:

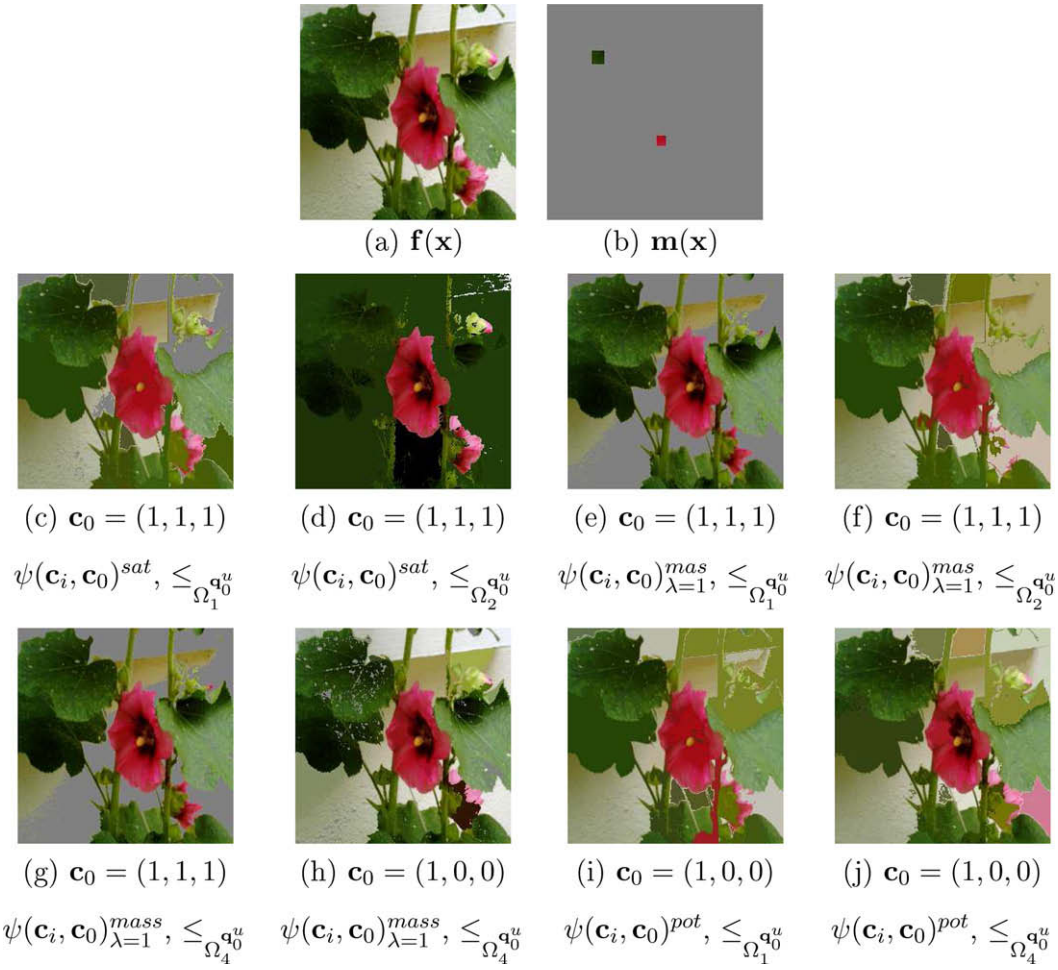

Fig. 8. Comparative of colour openings by reconstruction $\gamma^{rec}_{\Omega}(\mathbf{m},\mathbf{f})(\mathbf{x})$ on image "Flower 1" (the original image is (a) and the marker image is (b)) using different quaternionic orderings and with different scalar parts. (For interpretation of color mentioned in this figure the reader is referred to the web version of the article.)

Please cite this article in press as: J. Angulo, Geometric algebra colour image representations and derived total orderings for morphological operators – Part I: Colour quaternions, J. Vis. Commun. (2009), doi:10.1016/j.jvcir.2009.10.002

choosing the red, $\mathbf{c}_0 = (1, 0, 0)$ (Fig. 5(e)), the regions of middle greys and reddish colours are reduced.

A similar comparison is provided in Fig. 6. The image is a detail of the painting "Vincent's Bedroom in Arles" painted by V. Van Gogh in 1889. This case deals with a systematic comparison of colour closings, which typically roughly *regularise the structures*. Due to the properties of this particular painting, we have a large variety of colour in small regions and consequently, the results for the various operators are quite different. Hence, using the same reference (white colour), it is possible to identify the orderings which yield the best visual object regularisation and the colour nature of structures which are filtered. Orderings $\leqslant_{\Omega_0^{\mathbf{q}u}}$ and $\leqslant_{\Omega_0^{\mathbf{q}u}}$ lead to visual similar results for the three scalar parts with reference colour $\mathbf{c}_0 = (1, 1, 1)$, although this is not the case when other $\mathbf{c}_0$ are chosen. The mass scalar part gives smoother filtered images, independently from the ordering, in most of the studied cases. The effect in the various orderings of the scalar potential is limited to colour very close to the reference. It is perhaps interesting in future research to explore a potential function more asymmetric with respect to the values of positive and negative charges, and with a particular choice of the dominant colours for the negative charges.

The adjunction erosion/dilation can be used to build gradients. In the comparative of colour gradients of Fig. 7, by choosing as reference the colour of the skirt, $\mathbf{c}_0 = (0.40, 0.69, 0.96)$ we are sure that the morphological gradient associated to the ordering $\leqslant_{\Omega_0^{\mathbf{q}u}}$, $\psi(\mathbf{c}_i, \mathbf{c}_0)^{mass}$, catches the contours of the image, attributing more importance to the transitions between regions close/far to the reference colour. Besides to compare directly both gradients, we have used them to *segment the colour image* by hierarchical watershed transformation [28,29]. Using this algorithm we fix the number of significant regions to be segmented according to a volume criterion (i.e., a combination of the contrast and area of the region). As we can observe from the example, using adapted colour filtering regions around the skirt leads to a better segmentation than when no preference to colour is fixed (i.e., $c_0 = (1, 1, 1)$).

In order to illustrate the effect of geodesic colour propagations, Fig. 8 gives a comparison of colour "swamping": an opening by reconstruction of a function by imposing as markers the maxima associated to the objects to be preserved. These points initiate the propagation and the image is strongly simplified in such a way that the other image maxima are removed. For this example, the marker image is composed of a point on the red/pink flower and a point on one leaf. The background of the marker image should be set to the colours of the lower bound of each ordering. As we can observe, the most important property of these operators is their ability to preserve the image contours of objects. These different results show the strong possibilities of the various geodesic propagation types.

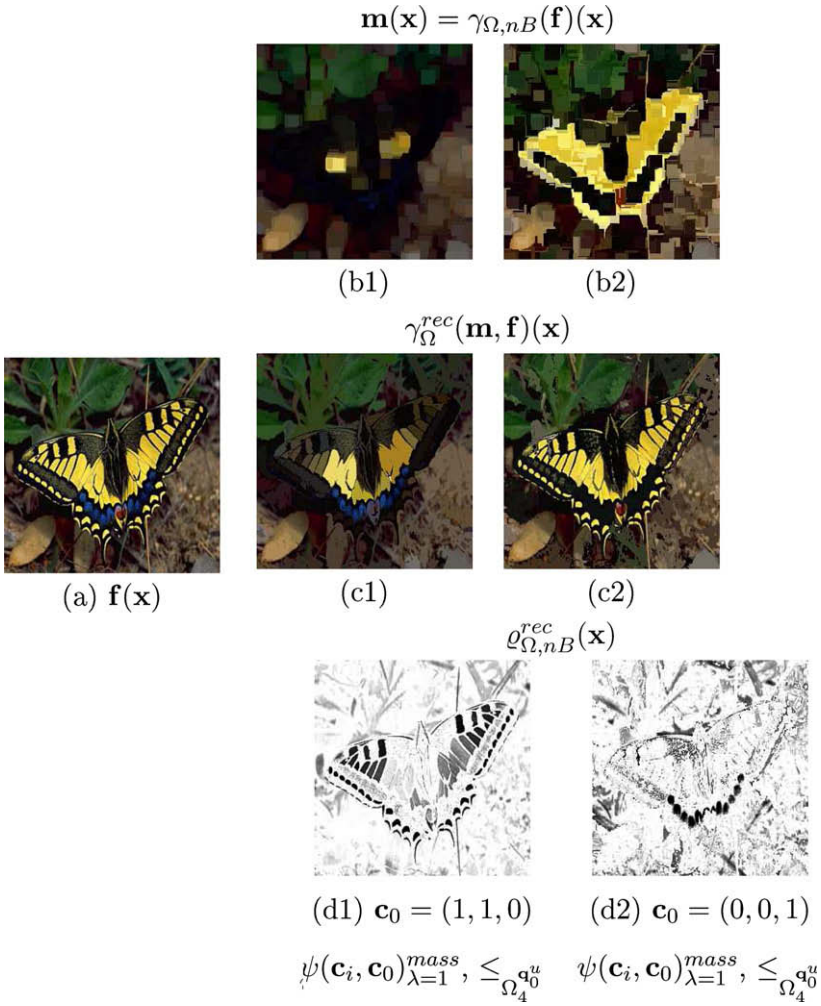

Fig. 9. Colour and size structure extraction using opening by reconstruction (c) of image "Butterfly 1" (a) with the same quaternionic total ordering and different reference colour $\mathbf{c}_0$. Markers are colour openings (b) of size $n = 12$ where the structuring element B is a disk. The negative of the residue is given in (d). See the text for more details. (For interpretation of color mentioned in this figure the reader is referred to the web version of the article.)

Please cite this article in press as: J. Angulo, Geometric algebra colour image representations and derived total orderings for morphological operators – Part I: Colour quaternions, J. Vis. Commun. (2009), doi:10.1016/j.jvcir.2009.10.002

Nevertheless, the excellent capabilities of geodesic operators to simplify selectively image structures do not require the introduction of manual markers for the target objects. Usually, the marker image is the result of an opening which removes the structures smaller than the size of the structuring element. Fig. 9 depicts an example of *colour/size structure extraction* just using an opening by reconstruction. Two different cases are provided, using the same total ordering $\leqslant_{\Omega_0^u}$ with mass as scalar part $\psi(\mathbf{c}_i, \mathbf{c}_0)_{\lambda=1}^{mass}$, and variation in the reference colour. By fixing the yellow, $c_0 = (1, 1, 0)$, the yellowish objects of size smaller than 12 are removed in the opening $\mathbf{m}(\mathbf{x}) = \gamma_{\Omega,nB}(\mathbf{f})(\mathbf{x})$, then the geodesic reconstruction using this opening as marker, $\gamma_\Omega^{rec}(\mathbf{m}, \mathbf{f})(\mathbf{x})$, restores the original contours of the yellow structures which still are connected to the colour structures of the marker image. By taking the residue between the original image and the reconstructed one, i.e., colour top-hat transformation $\varrho_{\Omega,nB}^{rec}(\mathbf{x}) = \|\mathbf{f}(\mathbf{x}) - \gamma_\Omega^{rec}(\mathbf{m}, \mathbf{f})(\mathbf{x})\|$, the removed details are detected. We notice that some small greenish details have been also simplified since their colour is close to yellow, whereas the blue small size structures are perfectly preserved. So, we can choose now the blue as the reference colour, $c_0 = (0, 0, 1)$, and apply the same transformations. The blue objects are removed by the opening (and the yellow ones fill the corresponding structures) and then by geodesic reconstruction the contours are recovered. Note that the blue spots on the butterfly wings have been suppressed. We observe also that some dark objects, closer to blue than to yellow, are also simplified by this transformation.

There are other very useful and classical applications of geodesic reconstruction in grey level images which are based on using an "image border" as marker. The counterpart in quaternionic colour morphology is a marker image, $\mathbf{m}(\mathbf{x})$ with a colour in the border and a background equal to the lower bound of the ordering. Let us illustrate this transformation with the comparative example of Fig. 10. In this case the reference colour is the blue $\mathbf{c}_0 = (0, 0, 1)$ and the same ordering is considered for the three cases. Using the blue border marker in a closing by reconstruction, $\varphi_\Omega^{rec}(\mathbf{m}, \mathbf{f})(\mathbf{x})$, with blue reference colour $\mathbf{c}_0 = (0, 0, 1)$ (Fig. 10(c3)), extract all the blue objects independently from their size or position in the image (some dark objects are also reconstructed). The marginal dual top-hat (i.e., an independent residue for each colour components), $\varphi_\Omega^{rec}(\mathbf{m}, \mathbf{f})(\mathbf{x}) - \mathbf{f}(\mathbf{x})$, produces the remaining colour objects (Fig. 10(d3)). Instead of a closing, we can also apply an opening by reconstruction $\gamma_\Omega^{rec}(\mathbf{m}, \mathbf{f})(\mathbf{x})$ in such a way that the selection of the reference colour allows to remove the bright/blue colours with $\mathbf{c}_0 = (1, 1, 1)$ (Fig. 10(c1)) and green colours with $\mathbf{c}_0 = (0, 1, 0)$ (Fig. 10(c2)); and then to extract the removed structures by the corresponding residue $\mathbf{f}(\mathbf{x}) - \gamma_\Omega^{rec}(\mathbf{m}, \mathbf{f})(\mathbf{x})$ (Fig. 10(d1) and (d2)). It is easy to see the potential applications of this simple family of transformations in order to *decompose the image into the background layer and the object layer*. Moreover, we remark again that the results of geodesic reconstruction for the colour quaternion-based ordering $\leqslant_{\Omega_4^{\mathbf{q}_0^u}, \psi(\mathbf{c}_i, \mathbf{c}_0)_{\lambda=1}^{mass}}$, are visually good independently of the reference colour.

5.1. Application to image-based traffic analysis

To conclude this section of results, we apply the colour quaternion operators introduced in the paper, and mainly the geodesic

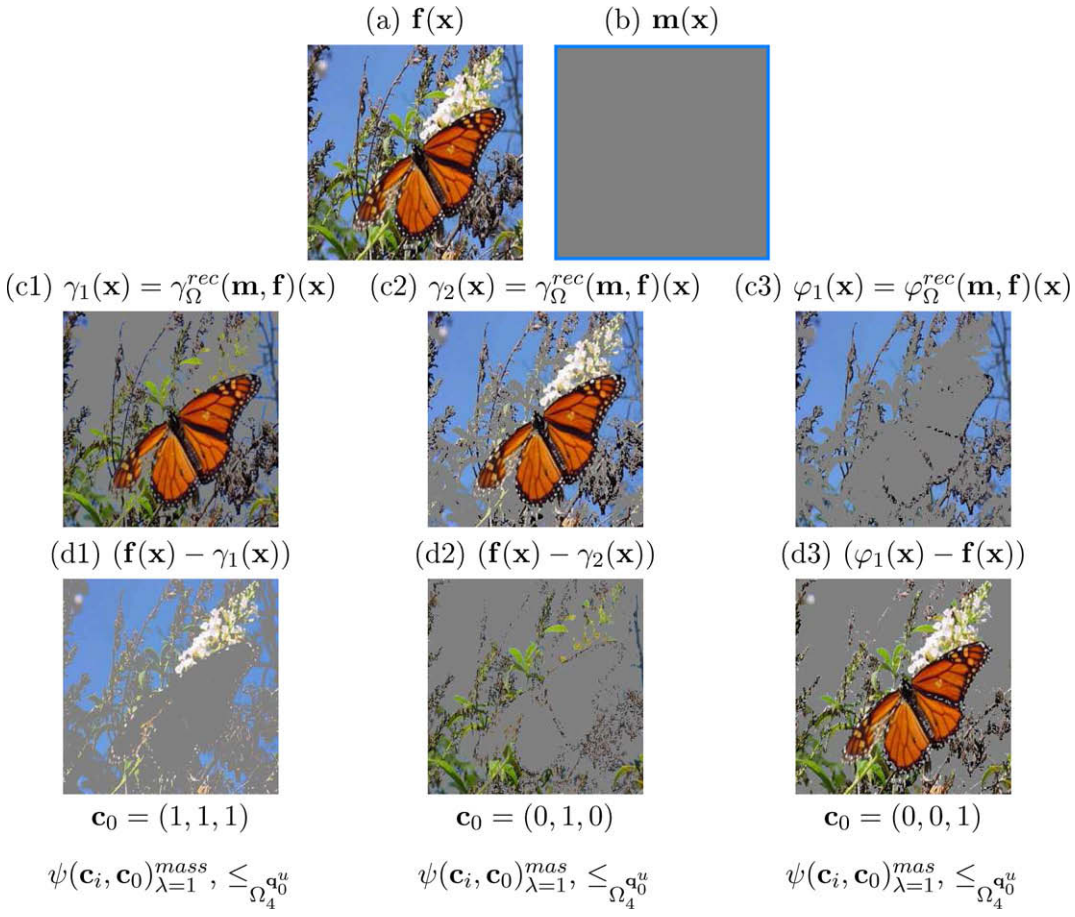

Fig. 10. Colour background + object decomposition using opening/closing by reconstruction of image "Butterfly 2" with the same quaternionic total ordering and different reference colour $\mathbf{c}_0$. The marker (b) is the image border set to colour (0, 0, 1). See the text for more details. (For interpretation of color mentioned in this figure the reader is referred to the web version of the article.)

Please cite this article in press as: J. Angulo, Geometric algebra colour image representations and derived total orderings for morphological operators – Part I: Colour quaternions, J. Vis. Commun. (2009), doi:10.1016/j.jvcir.2009.10.002

filters, for two applications in image-based traffic analysis. Our main motivation is just to show the usefulness of the proposed operators for the development of robust real life complex problems. In particular, the main advantage of the colour quaternion geodesic operators is the reduced number of parameters required for the algorithms.

5.1.1. Saliency detection in road images

Fig. 11(a) depicts two examples of natural road images acquired by an embarked car camera [43]. One of the classical applications of these images is the extraction of the more salient structures, i.e., the lane marking, the traffics signs and the interest zones of the cars. This problem can be easily solved using openings by reconstruction and in addition, using the colour quaternion representations, we can detect separately the bright structures and the red structures (these last elements correspond to warning signs or to tail lights). Given the original colour image $\mathbf{f}(\mathbf{x})$, the steps of the algorithm are:

(1) To compute a "white" opening by reconstruction (image (b) in Fig. 11): $\mathbf{f}_n^{white}(\mathbf{x}) = \gamma_{\Omega}^{rec}(\mathbf{m}^{white}, \mathbf{f})(\mathbf{x})$, where $\mathbf{m}^{white}(\mathbf{x}) = \gamma_{\Omega,nB}(\mathbf{f})(\mathbf{x})$ with $\mathbf{c}_0 = (1,1,1)$.
(2) To compute a "red" opening by reconstruction (image (c) in Fig. 11): $\mathbf{f}_n^{red}(\mathbf{x}) = \gamma_{\Omega}^{rec}(\mathbf{m}^{red}, \mathbf{f})(\mathbf{x})$, where $\mathbf{m}^{red}(\mathbf{x}) = \gamma_{\Omega,nB}(\mathbf{f})(\mathbf{x})$ with $\mathbf{c}_0 = (1,0,0)$.
(3) To define the salient bright zones as the colour residue of the corresponding opening (image (d) in Fig. 11): $\mathbf{s}_n^{white}(\mathbf{x}) = \mathbf{f}(\mathbf{x}) - \mathbf{f}_n^{white}(\mathbf{x})$.
(4) To define the salient red zones as colour the residue of the corresponding opening (image (e) in Fig. 11): $\mathbf{s}_n^{red}(\mathbf{x}) = \mathbf{f}(\mathbf{x}) - \mathbf{f}_n^{red}(\mathbf{x})$.
(5) To integrate both salient structure images in a global intensity saliency map (negative of the image (f) in Fig. 11): $\mathbf{s}_n(\mathbf{x}) = \|\mathbf{f}(\mathbf{x}) - \mathbf{f}_n^{white}(\mathbf{x})\| \vee \|\mathbf{f}(\mathbf{x}) - \mathbf{f}_n^{red}(\mathbf{x})\|$. This last step is necessary only if a single greylevel saliency map is required.

The images $\mathbf{s}_n^{white}$ and $\mathbf{s}_n^{red}$ can be then used as low-level features for a classification algorithm. We notice that only a parameter must be fixed: the size n of the structuring element for the openings, which correspond to the size of the largest structure of the image considered as a prominent object (as opposition to a background object).

5.1.2. Monitoring in traffic sequences

Video-based traffic monitoring is a classical issue in video sequence processing. It is needed, on the one hand, to detect the lane lines (active zones of the image) and on the other hand, to identify the cars driving in the road and the cars which are stopped. This last aim, which may indicate a situation of danger, cannot be detected

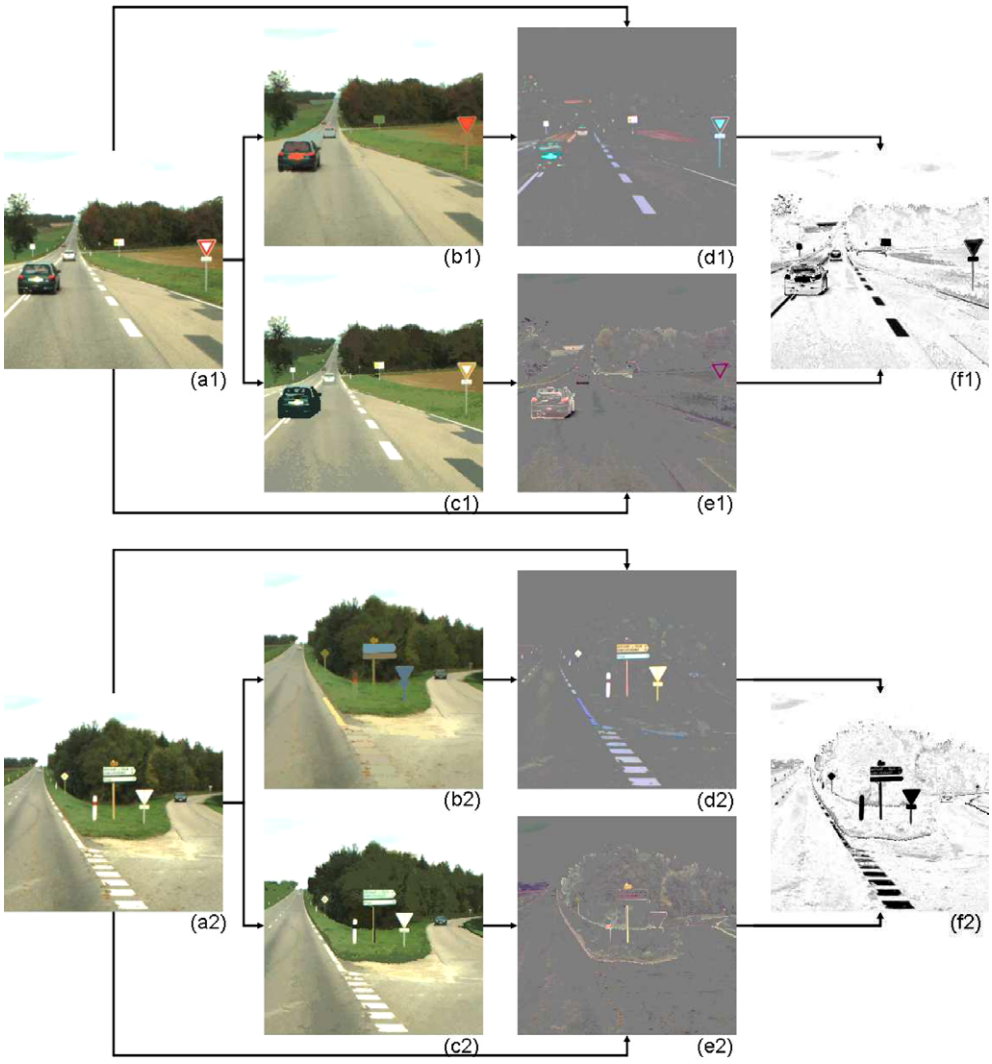

Fig. 11. Algorithm of saliency detection in road images (two examples from [43]): (a) original colour image, (b) colour opening by reconstruction on "white structures", (b) colour opening by reconstruction on "red structures", (d) salient bright zones, (e) salient red zones, and (f) integrated saliency map. See the text for more details.(For interpretation of color mentioned in this figure the reader is referred to the web version of the article.)

Please cite this article in press as: J. Angulo, Geometric algebra colour image representations and derived total orderings for morphological operators – Part I: Colour quaternions, J. Vis. Commun. (2009), doi:10.1016/j.jvcir.2009.10.002

by difference of successive frames. The proposed approach based again exclusively on colour quaternion openings/closings by reconstruction is illustrated in Fig. 12, and the steps are as follows.

(A) Initialization phase using frame $\sharp t_0$.
  (1) To compute the lane lines (image (b) in Fig. 12): closing by reconstruction followed by opening by reconstruction, i.e., $\mathbf{f}^{lane} = \gamma^{rec}_{\Omega}(\mathbf{m}^{white}, \varphi^{rec}_{\Omega}(\mathbf{m}^{white}, \mathbf{f}_{t_0}))$, where the marker image $\mathbf{m}^{white}(\mathbf{x})$ is an image border of value $\mathbf{c}_0 = (1,1,1)$, and the same reference colour is used for the corresponding ordering.
  (2) To compute the background layer of the scene, which is associated here to the vegetation (image (c) in Fig. 12): $\mathbf{f}^{bg} = \varphi^{rec}_{\Omega}(\mathbf{m}^{green}, \gamma^{rec}_{\Omega}(\mathbf{m}^{green}, \mathbf{f}_{t_0}))$, where the marker image $\mathbf{m}^{green}(\mathbf{x})$ is an image border of value $\mathbf{c}_0 = (0,1,0)$, and the same reference colour is used for the corresponding ordering.

(B) Running phase for frames $\sharp t_0, \sharp t_1, \sharp t_2, \ldots$ using the images $\mathbf{f}^{lane}$ and $\mathbf{f}^{bg}$.
  (1) To compute a simplified road image by removing secondary road marks (image (e) in Fig. 12): $\mathbf{f}^{*}_{t_i} = \gamma^{rec}_{\Omega}(\mathbf{m}^{white}, \mathbf{f}_{t_i})$, with $\mathbf{c}_0 = (1,1,1)$.
  (2) By difference with the background image, to obtain all the objects presented in the road (image (e) in Fig. 12): $\mathbf{o}^{all}_{t_i}(\mathbf{x}) = \|\mathbf{f}^{*}_{t_i}(\mathbf{x}) - \mathbf{f}^{bg}(\mathbf{x})\|$.
  (3) To obtain the objects in movement (negative of image (f) in Fig. 12): $\mathbf{o}^{mov}_{t_i}(\mathbf{x}) = \|\mathbf{o}^{all}_{t_{i-1}}(\mathbf{x}) - \mathbf{o}^{all}_{t_i}(\mathbf{x})\|$.

For the sake of simplicity, we have not included in the example how the lane lines image $\mathbf{f}^{lane}$ can be thresholded in order to obtain the binary mask of the main lines. The main lines may be used with image $\mathbf{o}^{all}_{t_i}$ the separate the objects of each line. The stopped red car of the example is well detected thanks to the soundness of the $\mathbf{f}^{bg}$. This last image can be periodically updated in order to cope for instance with strong illumination changes.

6. Conclusions and perspectives

In this paper we have studied the appropriateness of colour quaternion representations to extend mathematical morphology to colour images. To our knowledge this is the first work considering the definition of morphological operators using quaternions, and more generally, the first to define a complete lattice for quaternions.

From a methodological viewpoint this study has two main contributions. On the one hand, we have studied different alternatives to introduce the scalar part in order to obtain full colour quaternions. On the other hand, several lexicographic total orderings for quaternions based on their various decompositions have been defined. We conclude that the geometric and algebraic properties of quaternionic representations involve a rich structure to deal with ordering-based colour operations and it yields a powerful framework to generalise the definition of morphological operators for colour images.

We have illustrated with various examples the effects of basic morphological operators to process colour images. Then we have shown several cases of advanced morphological colour processing using connected operators (i.e., opening/closing by reconstruction) for colour/size feature extraction, colour object detection and background+object decomposition. From these tests we state that the ordering based on the decomposition into $\|/\perp$ parts is probably the most interesting ordering, although more exhaustive empirical tests are needed to qualitatively and quantitatively study the performances of all proposed orderings.

In addition, we believe that other quaternion-based colour operations (colour Fourier Transform, colour convolution, etc.),

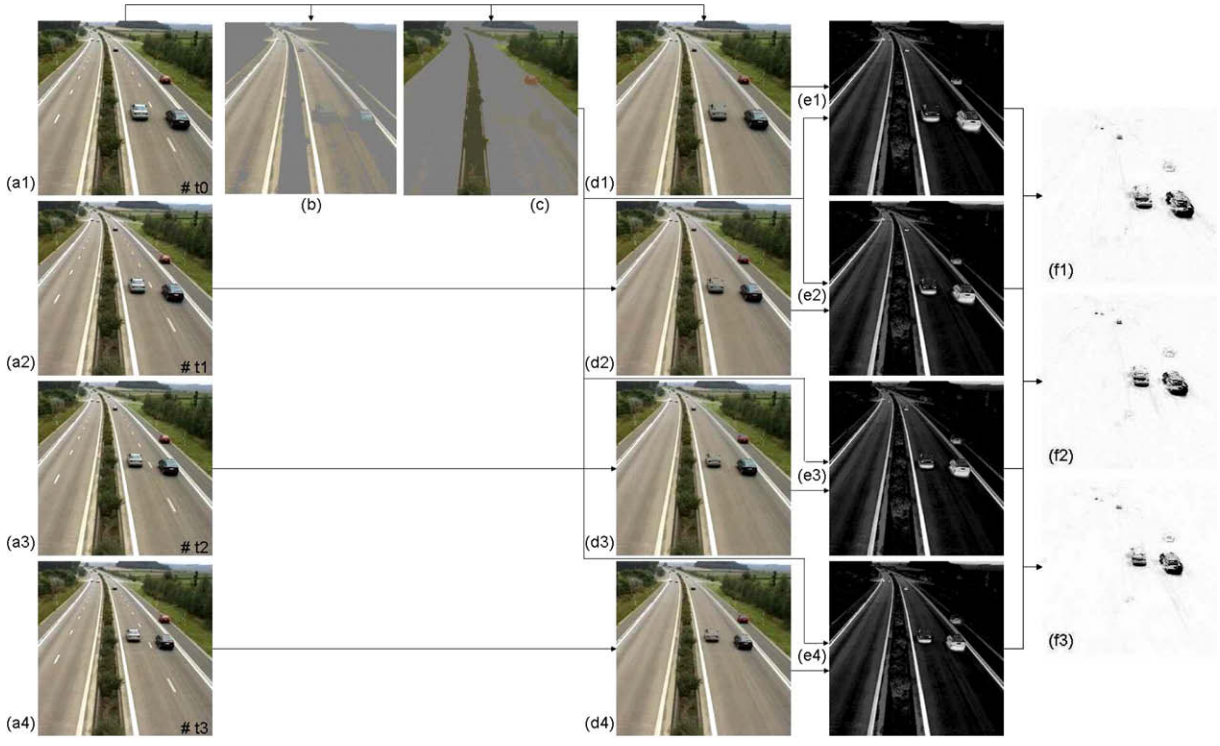

Fig. 12. Algorithm of monitoring traffic sequence (example with four time frames): (a) original colour image, (b) road extraction with main lanes, (c) background layer, (d) simplified image by removing secondary road marks, (e) objects included in the road, and (f) time difference between road objects. See the text for more details. (For interpretation of color mentioned in this figure the reader is referred to the web version of the article.)

Please cite this article in press as: J. Angulo, Geometric algebra colour image representations and derived total orderings for morphological operators – Part I: Colour quaternions, J. Vis. Commun. (2009), doi:10.1016/j.jvcir.2009.10.002

previously defined for pure colour quaternions, could be now studied for the full colour quaternions here proposed.

Two questions should be addressed in future studies. The first relates to the geometry of the colour space and the second to the generalisation to multispectral images. Since the basic R, G and B components are correlated in most images, the RGB space is not really orthogonal. It can be interesting to study how colour quaternions defined from uncorrelated basis C_1, C_2 and C_3, obtained by PCA of each image or using the uncorrelated colour representations proposed in the literature [30] or [46], perform in comparison with the results shown here. The extension to multispectral images (more than 3 spectral images) can be considered in the framework of Clifford algebras [22,1]. In fact, the $\|/\perp$ decomposition is defined for any Clifford algebra $\mathscr{G}_n$ or $\mathscr{G}_{n,m}$ according to the corresponding inner product.

As mentioned in Section 1, in the forthcoming second part of this paper we will consider colour mathematical morphology by introducing colour tensor representations and defining appropriate tensor total orderings.

Acknowledgments

The author gratefully thanks the reviewers for the valuable comments and improvements they suggested. Thanks are also addressed to Jean Serra for some stimulating discussions on multivariate mathematical morphology.

References

[1] R. Ablamowicz, P. Lounesto, J.M. Parra, Clifford Algebras with Numeric and Symbolic Computations, Birkhäuser, 1996.
[2] J. Angulo, J. Serra. Morphological coding of color images by vector connected filters, in: IEEE Proceedings of the Seventh International Symposium on Signal Processing and Its Applications (ISSPA'2003), vol. 1, Paris, 2003, pp. 69–72.
[3] J. Angulo, Morphological colour image simplification by saturation-controlled regional levellings, International Journal of Pattern Recognition and Artificial Intelligence 20 (8) (2006) 1207–1223.
[4] J. Angulo, J. Serra, Modelling and segmentation of colour images in polar representations, Image and Vision Computing 25 (4) (2007) 475–495.
[5] J. Angulo, Morphological colour operators in totally ordered lattices based on distances, application to image filtering, enhancement and analysis, Computer Vision and Image Understanding 107 (2 and 3) (2007) 56–73.
[6] E. Aptoula, S. Lefévre, A comparative study on multivariate morphology, Pattern Recognition 40 (11) (2007) 2914–2929.
[7] Ph. Carré, P. Denis, Quaternionic wavelet transform for colour images, in: Wavelet Applications in Industrial Processing IV, vol. 6383, Boston, USA, 2006.
[8] P. Denis, Ph. Carré, Ch. Fernandez-Maloigne, Spatial and spectral quaternionic approaches for colour images, Computer Vision and Image Understanding 107 (2 and 3) (2007) 74–87.
[9] S. Di Zenzo, A note on the gradient of a multi-image, Computer Vision, Graphics, and Image Processing 33 (1) (1986) 116–125.
[10] T.A. Ell, S.J. Sangwine, Hypercomplex Wiener-Khintchine theorem with application to color image correlation, in: IEEE ICIP'00, vol. II, 2000, pp. 792–795.
[11] T.A. Ell, S.J. Sangwine, Hypercomplex Fourier transform of color images, IEEE Transactions on Image Processing 16 (1) (2007) 22–35.
[12] T.A. Ell, S.J. Sangwine, Quaternion involutions and anti-involutions, Computers and Mathematics with Applications 53 (2007) 137–143.
[13] T.A. Ell, Hypercomplex color affine filters, in: Proceedings of the IEEE Conference on Image Processing (ICIP'07), vol. V, 2007, pp. 249–252.
[14] T.A. Ell, Multi-vectors color-image filters, in: Proceedings of the IEEE Conference on Image Processing (ICIP'07), vol. V, 2007, pp. 245–248.
[15] Th. Gevers, A.W.M. Smeulders, Color based object recognition, Pattern Recognition 32 (3) (1999) 453–464.
[16] C. Gomila, F. Meyer, Levelings in vector spaces, in: Proceedings of the IEEE Conference on Image Processing (ICIP'99), Kobe, Japan, October 24–28, 1999.
[17] J. Goutsias, H.J.A.M. Heijmans, K. Sivakumar, Morphological operators for image sequences, Computer Vision and Image Understanding 62 (3) (1995) 326–346.
[18] W.R. Hamilton, in: N. Halberstam, R.E. Ingram, The Mathematical Papers of Sir William Rowan Hamilton, vol. III, Cambridge University Press, Cambridge, 1967.
[19] A. Hanbury, Mathematical morphology in the HLS colour space, in: Proceedings of the 12th BMVC, British Machine Vision Conference, Manchester, 10–13 September 2001, pp. II-451–460.
[20] A. Hanbury, J. Serra, Morphological operators on the unit circle, IEEE Transactions on Image Processing 10 (12) (2001). 1842-Ũ1850.
[21] H.J.A.M. Heijmans, Morphological Image Operators, Academic Press, Boston, 1994.
[22] D. Hestenes, G. Sobczyk, Clifford algebra to geometric calculus: a unified language for mathematics and physics, D. Reidel, 1984.
[23] E. Labunets-Rundblad, V. Labunets, Spatial-colour clifford algebras for invariant image recognition, in: G. Sommer (Ed.), Geometric Computing with Clifford Algebra, Springer, 2001, pp. 155–185.
[24] E. Labunets-Rundblad, A. Maidan, P. Novak, V. Labunets, Fast color wavelet transforms, in: J. Byrnes, G. Ostheimer (Eds.), Computational Noncommutative Algebra & Applications, NATO Sciences Series II Mathematics, Physics & Chemistry, vol. 136, Kluwer, 2003, pp. 401–412.
[25] V. Labunets, Clifford Algebras as Unified Language for Image Processing and Pattern Recognition, in: J. Byrnes, G. Ostheimer (Eds.), Computational Noncommutative Algebra & Applications, NATO Sciences Series II Mathematics, Physics & Chemistry, vol. 136, Kluwer, 2003.
[26] N. Le Bihan, S.J. Sangwine, Quaternion principal component analysis of color images, in: Proceedings of the International Conference on Image Processing (ICIP'03), vol. 1, 2003, pp .809–812.
[27] G. Matheron, Les treillis compacts, Technical Report-Paris School of Mines, N-23/90/G, November 1990.
[28] F. Meyer, S. Beucher, Morphological segmentation, Journal of Visual Communication and Image Representation 1 (1) (1990) 21–45.
[29] F. Meyer, An overview of morphological segmentation, International Journal of Pattern Recognition and Artificial Intelligence 15 (7) (2001) 1089–1118.
[30] Y-I. Ohta, T. Kanade, T. Sakai, Color information for region segmentation, Computer Graphics and Image Processing 13 (1980) 222–241.
[31] S.-C. Pei, C.-M. Cheng, Color image processing by using binary quaternion-moment-preserving thresholding technique, IEEE Transactions on Image Processing 8 (5) (1999) 614–628.
[32] S.-C. Pei, J.-H. Chang, J.-J. Ding, Quaternion matrix singular value decomposition and its applications for color image processing, in: Proceedings of the International Conference on Image Processing (ICIP'03), vol. 1, 805–808, 2003.
[33] Ch. Poynton, in: Digital Video and HDTV-Algorithms and Interfaces, Morgan Kaufmann, Elsevier Science, San Francisco, 2003.
[34] S.J. Sangwine, Fourier transforms of colour images using quaternion, or hypercomplex, numbers, Electronics Letters 32 (21) (1996) 1979–1980.
[35] S.J. Sangwine, Colour image edge detector based on quaternion convolution, Electronics Letters 34 (10) (1998) 969–971.
[36] S.J. Sangwine, T.A. Ell, Mathematical approaches to linear vector filtering of colour images, in: Proceedings of the European Conference on Colour in Graphics, Imaging and Vision (CGIV'02), 2002, vol. 348–351.
[37] J. Serra, Image Analysis and Mathematical Morphology, vol. I, Academic Press, London, 1982; Image Analysis and Mathematical Morphology: Theoretical Advances, vol. II, Academic Press, London, 1988.
[38] J. Serra, Anamorphoses and Function Lattices (Multivalued Morphology), in: Dougherty (Ed.) Mathematical Morphology in Image Processing, Marcel-Dekker, 1992, pp. 483–523.
[39] L. Shi, B. Funt, Quaternion color texture segmentation, Computer Vision and Image Understanding 107 (1 and 2) (2007) 88–96.
[40] N. Sochen, Y.Y. Zeevi, Representation of colored images by manifolds embedded in higher dimensional non-Euclidean space, in: Proceedings of the International Conference on Image Processing (ICIP'98), vol. 1, 1998, pp. 166–170.
[41] N. Sochen, R. Kimmel, R. Malladi, A general framework for low level vision, IEEE Transactions on Image Processing 7 (3) (1998) 310–318.
[42] H. Talbot, C. Evans, R. Jones. Complete ordering and multivariate mathematical morphology: algorithms and applications, in: Proceedings of the International Symposium on Mathematical Morphology (ISMM'98), Kluwer, 1998, pp. 27–34.
[43] T. Veit, J.-P. Tarel, P. Nicolle, P. Charbonnier, Evaluation of road marking feature extraction, in: Proceedings of the 11th IEEE Conference on Intelligent Transportation Systems (ITSC'08), Beijing, China, October 12–15, 2008.
[44] L. Vincent, Morphological grayscale reconstruction in image analysis: applications and efficient algorithms, IEEE Transactions on Image Processing 2 (2) (1993) 176–201.
[45] G. Wyszecki, W.S. Stiles, Color Science: Concepts and Methods, Quantitative Data and Formulae, second ed., John Wiley & Sons, New-York, 1982.
[46] S. Wolf, R. Ginosar, Y.Y. Zeevi, Spatio-chromatic image enhancement based on a model of human visual information processing, Journal of Visual Communication and Image Representation 9 (1) (1998) 25–37.

Please cite this article in press as: J. Angulo, Geometric algebra colour image representations and derived total orderings for morphological operators – Part I: Colour quaternions, J. Vis. Commun. (2009), doi:10.1016/j.jvcir.2009.10.002